THE ASTROPHYSICAL JOURNAL, 499:234–249, 1998 May 20
© 1998. The American Astronomical Society. All rights reserved. Printed in U.S.A.

THE IONIZATION FRACTION IN DENSE CLOUD CORES

P. CASELLI AND C. M. WALMSLEY
Osservatorio Astrofisico di Arcetri, Largo E. Fermi 5, I-50125 Firenze, Italy; caselli@arcetri.astro.it, walmsley@arcetri.astro.it
R. TERZIEVA
Chemical Physics Program, Ohio State University, Columbus, OH 43210; terzieva@mps.ohio-state.edu
AND
ERIC HERBST
Departments of Physics and Astronomy, Ohio State University, Columbus, OH 43210; herbst@mps.ohio-state.edu
Received 1997 August 13; accepted 1998 January 2

ABSTRACT

The degree of ionization, $x(e) = n(e)/n(H_2)$, and the cosmic-ray ionization rate, ζ, in 24 cloud cores have been determined by comparing observational data from Butner et al. on the abundance ratios $R_D = [DCO^+]/[HCO^+]$ and $R_H = [HCO^+]/[CO]$ with a simple analytical chemical model and with a detailed "pseudo–time-dependent" chemical model. The results are dependent on the depletion of elemental carbon and oxygen from their cosmic abundances, especially for cores with a low degree of ionization. We determine the depletion of C and O from the measured HC_3N/CO abundance ratios using model results. We find that the range of fractional ionization in the dark cores extends from $\sim 10^{-6}$ to $\sim 10^{-8}$, with inferred cosmic ray ionization rates in the range of 10^{-16}–10^{-18} s^{-1}. This corresponds to ambipolar diffusion timescales of between 3×10^7 and 3×10^5 yr, with a median value of 5×10^6 yr. The ratio of ambipolar diffusion to the free-fall timescales varies between 3 and 200, with a median value of 50. We find, rather surprisingly, no clear segregation in the ambipolar diffusion timescales between cores with embedded stars and those without. An interesting by-product of our results is the conclusion that the cyanopolyyne-rich core in TMC-1 is atypical in its abundance distribution and may be unusually young.

Subject headings: cosmic rays — diffusion — ISM: abundances — ISM: clouds — molecular processes

1. INTRODUCTION

The degree of ionization in dense cores of molecular clouds is thought to be the fundamental parameter regulating the rate of star formation. This is due to the process of ambipolar diffusion, whereby the neutral particles in dense cores of low ionization [$n(e)/n_H \sim 10^{-7}$, where $n(e)$ is the electron density and $n_H = n(H) + 2n(H_2)$ is the hydrogen density] contract relative to the magnetic field and the ionized component. The timescale for this process (see Spitzer [1978] and Shu, Adams, & Lizano [1987] for discussions) is roughly $2.5 \times 10^{13} x(e)$ yr [$x(e) = n(e)/n(H_2)$], or a few times the free-fall timescale in dense cores [$4 \times 10^7 (n_H)^{-1/2}$ yr] for typical densities of $n_H \sim 10^5$ cm^{-3}. The ratio of ambipolar diffusion to free-fall times thus depends sensitively on the degree of ionization, and this in turn depends on the poorly known cosmic-ray flux and metal depletion within the cores.

Observational determinations of the fractional ionization in nearby dense cores are thus of considerable interest. One obvious approach is to determine abundances for molecular ions such as HCO^+, N_2H^+, etc. In certain extreme situations, such species can become a major repository of positive charge. However, it seems probable that in most cases of interest, atomic ions such as C^+, Mg^+, Fe^+, etc., have abundances comparable to or larger than those of the molecular ions, and we do not in general have methods for directly determining the abundances of the atomic ions. In this situation, the best hope for determining the electron abundance is on the basis of measured molecular column densities sensitive to the electron density; thus, there have been a variety of attempts to derive the ionization degree from the observed chemistry (Langer 1985).

In particular, there have been attempts in the past to use either the observed degree of deuterium fractionation (Guélin, Langer, & Wilson 1982; Dalgarno & Lepp 1984; Wootten, Loren, & Snell 1982) or the abundances of selected molecular ions (de Boisanger, Helmich, & van Dishoeck 1996) to determine $x(e)$. In general, however, these have not made use of the results of detailed chemical modeling (e.g., Millar, Bennett, & Herbst 1989; Bettens, Lee, & Herbst 1995; Caselli, Hasegawa, & Herbst 1994), which have become increasingly sophisticated over the years. Moreover, work in the past has usually made use of one particular abundance ratio (e.g., $[DCO^+]/[HCO^+]$) in order to derive $x(e)$. This can be dangerous, since each indicator of electron abundance is influenced by a variety of other parameters; it is only by using two or more independent measures that one can get some assurance that the results are reliable.

This work is an attempt to improve the reliability of ionization determinations in dense cores. It has been partially inspired by the work of Butner, Lada, & Loren (1995), who have supplied determinations of both the $[DCO^+]/[HCO^+]$ and the $[HCO^+]/[CO]$ abundance ratios for a large sample of nearby dense cores. We attempt to fit the data of Butner et al. with the pseudo–time-dependent models of Lee, Bettens, & Herbst (1996), varying the density, the cosmic-ray ionization rate ζ, the refractory metal abundances, and the C and O depletions in an attempt to find reasonable agreement with the Butner et al. (1995) data. We then use our results to estimate the degree of ionization in the cores studied by Butner et al. Finally, we consider the consequences of our results for the ambipolar diffusion timescales in these objects.

2. OBSERVATIONAL DATA

A variety of observations have been taken with a view to understanding the variation of ionization in dense clouds (Guélin et al. 1982; Wootten et al. 1982; de Boisanger et al. 1996). The most homogeneous data set available is that of Butner et al. (1995, hereafter BLL), who observed $C^{18}O$, $H^{13}CO^+$, and DCO^+ in a sample of 24 dark cores. These objects were essentially all observed by Benson & Myers (1989) in ammonia and have temperatures close to 10 K. The average H_2 number densities derived from column densities and size estimates are on the order of 10^4 cm^{-3}, although densities based on the relative intensities of the DCO^+ (1–0), (2–1), and (3–2) transitions are typically a factor of 5 higher.

BLL have determined the abundance ratios $R_D = [DCO^+]/[HCO^+]$ and $R_H = [HCO^+]/[CO]$. We can thus plot their results in a two-dimensional diagram, as shown in Figure 1, and compare these with model predictions (discussed in the next sections). Although some of the assumptions made by BLL (e.g., LTE at 10 K) are debatable, tests that we have made suggest that their estimates of R_H are good to a factor of 1.3 and that their estimates of R_D are not affected by the assumption of LTE, given that the same excitation temperature has been adopted for the calculation of the DCO^+ and $H^{13}CO^+$ column densities. The observed values of R_D lie in the range 0.025–0.07 (typical errors are ± 0.15 dex; see Fig. 1). Comparing this with the interstellar D/H ratio of 1.5×10^{-5}, we conclude that deuterium is enriched by factors between 1000 and 5000. On the other hand, the observed values of R_H lie in the range 2×10^{-5} to 10^{-4}. This is an order of magnitude less than the values derived by Lucas & Liszt (1996) toward diffuse clouds observed in absorption, which presumably is a reflection of the influence of the radiation field on the chemistry in the diffuse regions. We also note that BLL estimated $C^{18}O$ column densities in the range of 7×10^{14} to 4×10^{15} cm^{-2}, corresponding to visual extinctions A_V between 2 and 12 mag. McKee (1989, eq. [4.6]) estimates that photoionization becomes negligible for A_V greater than 3 mag in the density range of interest to us, suggesting that the ionization in the cores of the objects under study here is mainly influenced by cosmic rays and not by the ambient radiation field.

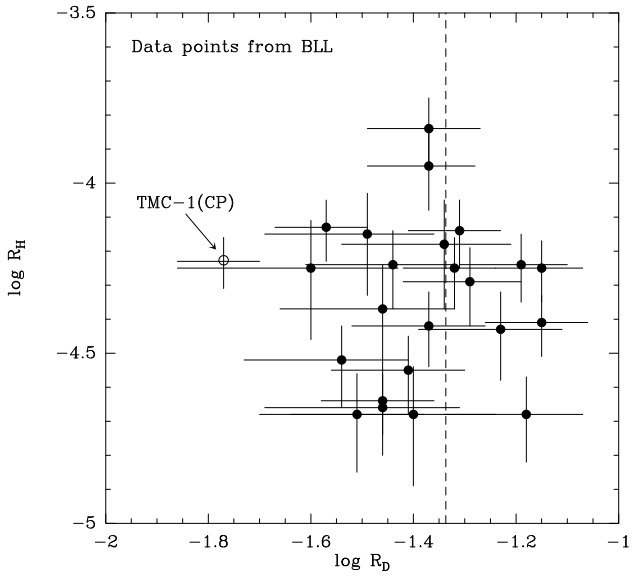

FIG. 1.—Observed $R_H \equiv [HCO^+]/[CO]$ abundance ratios as a function of $R_D \equiv [DCO^+]/[HCO^+]$ in low-mass cores (from Butner et al. 1995; BLL). Error bars (1 σ) have been computed on the basis of the uncertainties in the line intensities given by BLL. The observed ranges of the two quantities are: $0.025 \leq R_D \leq 0.07$, with the exception of TMC-1 (CP) (*open circle*), where $R_D = 0.017$; and $2 \times 10^{-5} \leq R_H \leq 1.6 \times 10^{-4}$. Electron fraction and cosmic-ray ionization rate can be analytically determined only for those cores with R_D less than 0.046 (*dashed line*), if carbon and oxygen are depleted by a factor of 2 (see § 3).

However, taken at face value this would indicate that a considerable fraction of the BLL cores are penetrated by radiation (and the referee has emphasized this point). We do not in fact think that UV radiation penetrates the regions sampled by BLL, because we consider it likely that the BLL column density estimates based on $C^{18}O$ are underestimates. One reason for this is the discrepancy mentioned above between densities derived from DCO^+ and mean densities derived from $C^{18}O$. Another reason is that our results (see § 5.2) indicate that CO is partially depleted out onto grain surfaces, and that consequently the H_2 column densities derived from $C^{18}O$ are underestimates (by factors of ~ 2). Finally and most importantly, we note that for a few of the BLL cores, there are 1.3 mm estimates of the dust column density available (Ward-Thompson et al. 1994). For the cores L63 and L183, these authors derive H_2 column densities on the order of 2×10^{23} cm^{-2}, or roughly 40 times more than the BLL estimates based on $C^{18}O$. While there are considerable uncertainties in all of the above estimates, we conclude from this that the BLL $C^{18}O$-derived column densities are underestimates by at least a factor of 2. Thus, the visual extinctions range upward from a lower limit of 4 mag to values perhaps as large as 200 mag, and one can neglect the radiation field in the dense regions of the clouds sampled by DCO^+ and HCO^+. We note incidentally that we initially computed some models that include the effects of an external UV radiation field and were unable to reproduce the results displayed in Figure 1. We thus ignore such effects in the rest of this article.

There may be differences in the spatial distributions of the tracers used by BLL, due to both inhomogeneity and abundance gradients. $C^{18}O$, for example, is known to be more extended than ammonia and CS toward many cores (see, e.g., Myers et al. 1991). Thus, one might argue that $H^{13}CO^+$, DCO^+, and $C^{18}O$ are not spatially coexistent and that hence the ratios R_H and R_D are meaningless. However, as noted above, we do not expect the influence of UV penetration of these cores to be important, and hence gradients between exterior layers where UV ionization dominates and central regions where cosmic-ray ionization dominates should be negligible. We (Caselli et al., in preparation) have moreover made observations of one core (L1544) with the IRAM 30 m telescope that show essential agreement between the spatial distributions of $H^{13}CO^+$ (1–0) and DCO^+ (2–1). It is also worth noting that ^{13}C fractionation of $H^{13}CO^+$ is unlikely to be important because of the close chemical links between HCO^+ and CO (CO cannot easily be fractionated because it is a major repository of gas-phase carbon). These arguments taken together lead us to the conclusion that R_D is at least a well-determined quantity for the BLL sample to within the error bars shown in Figure 1. The situation is less clear for R_H, and we suspect that $H^{13}CO^+$ is more concentrated in high-density regions than $C^{18}O$. This would cause the R_H

estimates of BLL to be lower limits. It turns out (see § 5) that our ionization degree estimates are more sensitively dependent upon R_D than R_H, and we therefore feel justified in ignoring such effects presently. However, future studies should certainly bear this problem in mind.

We have examined the BLL data for possible trends or correlations between the observed quantities. An anti-correlation between $C^{18}O$ column density and the HCO^+/CO abundance ratio is evident in the Butner et al. (1995) data. A linear fit to the data gives the relation $\log N(C^{18}O) = (13.7 \pm 0.7) - (0.36 \pm 0.17) \log R_H$, with a correlation coefficient $R = 0.42$. This implies an increase of HCO^+ fractional abundance toward regions of lower A_V. On the other hand, no correlation is found between $N(C^{18}O)$ and R_D.

We find a very weak correlation ($R = 0.18$) between the observed DCO^+ line width and R_D. Charnley & Roberge (1992) have suggested that deuterated ions may be destroyed by nonthermal reactions with neutrals in turbulent regions of dark clouds where magnetohydrodynamic (MHD) waves are propagating. In particular, ion-neutral streaming resulting from ambipolar diffusion allows the reaction $H_2D^+ + H_2 \rightarrow H_3^+ + HD$ to proceed at a fast nonthermal rate, quenching the deuteration process. However, Charnley & Butner (1995) also noted that the DCO^+ abundance is less affected by turbulence than other ions, such as N_2D^+. We have decided to neglect reactions of this type in our analysis, based both on the observed weak correlation and the theoretical results of Charnley & Butner.

It is also worth noting that a lower value of R_D has been observed toward the "cyanopolyyne peak" of TMC-1 (TMC-1[CP] in Figure 1; Guélin et al. 1982). TMC-1 (CP) is outstanding for its chemical composition, characterized by high fractional abundances of complex carbon-bearing molecules, in particular long carbon chain species (Irvine, Goldsmith, & Hjalmarson 1987; Pratap et al. 1997). Given that this source is often used as a typical dark cloud for the purpose of abundance comparisons, it is interesting that the observed value of R_D is so low. We consider this further in the following discussion.

3. ANALYTIC DETERMINATION OF $x(e)$

A variety of simple models (see, e.g., Langer 1985; Dalgarno & Lepp 1984) have been developed to estimate the ionization fraction and cosmic-ray ionization rate in molecular clouds. Many of the numerical results are easily understood on the basis of the analytical formulae, and we therefore recapitulate these results here. In a simple steady-state model, the $[DCO^+]/[HCO^+]$ ($\equiv R_D$) and $[HCO^+]/[CO]$ ($\equiv R_H$) abundance ratios are given by (see, e.g., Wootten, Snell, & Glassgold 1979; Guélin et al. 1982):

$$R_D = \frac{1}{3}\frac{k_f\, x(\mathrm{HD})}{k_e\, x(e) + \delta} \tag{1}$$

$$R_H = \frac{[\zeta/n(H_2)]k_{H_3^+}}{[\beta x(e) + \delta]\beta' x(e)}, \tag{2}$$

where k_f is the forward rate coefficient for the exchange reaction $H_3^+ + HD \leftrightarrow H_2D^+ + H_2$ (see Table 2), k_e is the dissociative recombination rate of H_2D^+ (Table 2), $\beta = 1.15 \times 10^{-7}(T/300)^{-0.65}$ cm^3 s^{-1} (M. Larsson 1997, private communication) is the dissociative recombination rate coefficient of H_3^+, $\beta' = 2.0 \times 10^{-7}(T/300)^{-0.75}$ cm^3 s^{-1} is the dissociative recombination rate coefficient of HCO^+, $k_{H_3^+} = 6.56 \times 10^{-10}(T/300)^{-0.5}$ cm^3 s^{-1} is the rate coefficient for the reaction $H_3^+ + CO \rightarrow HCO^+ + H_2$, $x(\mathrm{HD}) \sim 3 \times 10^{-5}$ is the fractional abundance of HD relative to H_2 (Linsky et al. 1995), and ζ is the cosmic-ray

TABLE 1

ELECTRON FRACTIONS AND COSMIC-RAY IONIZATION RATES FROM ANALYTICAL METHOD

	$f_D = 2$		$f_D = 3$		$f_D = 5$	
CORE	$\log x(e)_a$	$\log \zeta_a$	$\log x(e)_a$	$\log \zeta_a$	$\log x(e)_a$	$\log \zeta_a$
B5	−6.56	−15.41	**−6.32**	**−15.10**	−6.20	−14.93
L1489	...	...	−6.82	−15.54	**−6.51**	**−15.14**
L1495	−7.11	−16.03	**−6.56**	**−15.38**	−6.36	−15.12
L1551–IR	...	...	**−8.06**	**−17.34**	−6.77	−15.92
L43	...	...	**−6.78**	**−15.50**	−6.49	−15.12
B335	−6.75	−15.65	**−6.42**	**−15.25**	−6.27	−15.04
L1174	−6.63	−15.58	**−6.36**	**−15.24**	−6.23	−15.05
L1172	−6.32	−14.61	−6.17	−14.41	**−6.08**	**−14.28**
L1262	...	...	...	...	−6.85	−15.37
B217	...	...	−6.90	−15.40	−6.54	−14.95
TMC-2A	...	...	**−7.74**	**−17.06**	−6.75	−15.94
L1536	...	...	**−7.23**	**−16.60**	−6.66	−15.89
TMC-1C	−6.47	−15.91	−6.27	−15.65	**−6.16**	**−15.50**
L234A	−7.48	−16.22	−6.63	−15.26	**−6.40**	**−14.96**
L234E	−6.84	−15.56	**−6.46**	**−15.09**	−6.30	−14.87
L1498	−6.75	−15.56	−6.42	−15.16	**−6.27**	**−14.95**
L1400G	...	...	−6.72	−16.43	−6.46	−16.09
TMC-2	−7.48	−16.80	−6.63	−15.84	**−6.41**	**−15.54**
TMC-1	−6.39	−14.60	−6.22	−14.37	**−6.12**	**−14.23**
L134A	−6.75	−15.73	**−6.42**	**−15.33**	−6.27	−15.12
L183	−7.03	−16.86	−6.53	−16.31	**−6.34**	**−16.06**
L1696A	−7.48	−16.23	−6.63	−15.27	−6.41	−14.97
L63	...	...	...	...	−6.85	−16.01
TMC-1 (CP)	−6.00	−14.33	−5.92	−14.22	**−5.87**	**−14.14**

NOTE.—Numbers in boldface represent the best estimate of $x(e)$ and ζ after determining f_D (see text).

TABLE 2

IMPORTANT DEUTERATION REACTIONS INCLUDED IN THE LBH MODEL

Reaction	A ($cm^3\ s^{-1}$)	B	C (K)
$H^+ + HD \rightarrow D^+ + H_2$	1.00×10^{-9}	0.0	464
$D^+ + H_2 \rightarrow H^+ + HD$	2.10×10^{-9}	0.0	0.0
$H_3^+ + D \rightarrow H_2D^+ + H$	1.00×10^{-9}	0.0	0.0
$H_3^+ + HD \rightarrow H_2D^+ + H_2$	1.50×10^{-9}	0.0	0.0
$H_2D^+ + H_2 \rightarrow H_3^+ + HD$	2.00×10^{-9}	−0.8	230
$H_2D^+ + CO \rightarrow HCO^+ + HD$	4.00×10^{-10}	−0.5	0.0
$H_2D^+ + CO \rightarrow DCO^+ + H_2$	2.00×10^{-10}	−0.5	0.0
$H_2D^+ + N_2 \rightarrow N_2D^+ + H_2$	5.66×10^{-10}	0.0	0.0
$H_2D^+ + N_2 \rightarrow N_2H^+ + HD$	1.13×10^{-9}	0.0	0.0
$H_2D^+ + CH_4 \rightarrow CH_4D^+ + H_2$	8.00×10^{-10}	0.0	0.0
$H_2D^+ + CH_4 \rightarrow CH_5^+ + HD$	1.60×10^{-9}	0.0	0.0
$CH_2^+ + HD \rightarrow CH_3^+ + D$	3.60×10^{-10}	0.0	0.0
$CH_2^+ + HD \rightarrow CH_2D^+ + H$	3.60×10^{-10}	0.0	0.0
$HCO^+ + D \rightarrow DCO^+ + H$	1.00×10^{-9}	0.0	0.0
$DCO^+ + H \rightarrow HCO^+ + D$	2.20×10^{-9}	0.0	796
$N_2H^+ + D \rightarrow N_2D^+ + H$	1.00×10^{-9}	0.0	0.0
$N_2D^+ + H \rightarrow N_2H^+ + D$	2.20×10^{-9}	0.0	550
$C_2H_2^+ + HD \rightarrow C_2HD^+ + H_2$	1.00×10^{-9}	0.0	0.0
$C_2HD^+ + H_2 \rightarrow C_2H_2^+ + HD$	2.50×10^{-9}	0.0	550
$CH_3^+ + HD \rightarrow CH_2D^+ + H_2$	1.30×10^{-9}	0.0	0.0
$CH_2D^+ + H_2 \rightarrow CH_3^+ + HD$	8.70×10^{-9}	0.0	370
$CH_4D^+ + CO \rightarrow DCO^+ + CH_4$	3.20×10^{-10}	−0.5	0.0
$H + OD \rightarrow OH + D$	1.30×10^{-10}	0.0	810
$D + OH \rightarrow OD + H$	1.30×10^{-10}	0.0	0.0
$H_2D^+ + e \rightarrow H + H + D$	4.38×10^{-8}	−0.65	0.0
$H_2D^+ + e \rightarrow H_2 + D$	4.20×10^{-9}	−0.65	0.0
$H_2D^+ + e \rightarrow HD + H$	1.20×10^{-8}	−0.65	0.0
$N_2D^+ + e \rightarrow N_2 + D$	1.70×10^{-7}	−0.90	0.0
$DCO^+ + e \rightarrow CO + D$	2.00×10^{-7}	−0.75	0.0
$C_2HD^+ + e \rightarrow C_2 + D + H$	2.00×10^{-7}	−0.5	0.0
$C_2HD^+ + e \rightarrow C_2H + D$	1.00×10^{-7}	−0.5	0.0
$CH_2D^+ + e \rightarrow CH + HD$	5.00×10^{-7}	−0.5	0.0
$CH_4D^+ + e \rightarrow CH_3 + HD$	2.20×10^{-7}	−0.3	0.0
$CH_4D^+ + e \rightarrow CH_4 + D$	1.10×10^{-7}	−0.3	0.0

NOTE.—The rate coefficients k are given in the standard form for collisional processes: $k = A\,(T/300)^B \exp(-C/T)$, where T is the gas kinetic temperature.

ionization rate. The term $\delta = \delta_{H_2D^+} \sim \delta_{H_3^+}$ is the destruction rate for H_2D^+ and H_3^+ due to reactions with neutral species such as CO and O.

From equations (1) and (2) we can calculate $x(e)$ and ζ, after making an estimate of δ. Model calculations (see Lee, Bettens, & Herbst 1996; hereafter LBH) show that at steady state, gas-phase carbon is essentially in the form of CO and the residual oxygen is atomic. In this situation, one has $x(O) \sim x(CO) = 1.5 \times 10^{-4}$ for the choice of O and C abundances adopted by LBH. In a situation where, because of depletion onto dust grain surfaces, only a fraction $1/f_D$ of the O and C (relative to the LBH values) remains in the gas phase, one finds that the H_3^+ destruction rate at 10 K is $\delta = 6.5 \times 10^{-13}/f_D\ cm^3\ s^{-1}$.

By substituting the above numerical values into equations (1) and (2), we obtain two simple expressions that allow a direct estimate of $x(e)$ and the cosmic-ray ionization rate ζ at 10 K as

$$x(e) = \frac{2.7 \times 10^{-8}}{R_D} - \frac{1.2 \times 10^{-6}}{f_D}, \quad (3)$$

$$\zeta = \left[7.5 \times 10^{-4} x(e) + \frac{4.6 \times 10^{-10}}{f_D}\right] x(e) n(H_2) R_H . \quad (4)$$

We note that the first term on the right-hand side of equation (3) differs by a factor of order 5 from the corresponding term in the work of Guélin, Langer, & Wilson (1982), a result of the fact that we use more recent rate coefficients and consequently derive higher estimates of $x(e)$ than they do. From equation (3) it is clear that R_D values greater than a critical value $R_{Dc} = 0.023 \times f_D$ cannot be accounted for in the framework of this simple model (cf. Dalgarno & Lepp 1984). Thus, for the sources in Figure 1 with the largest values of R_D (~ 0.07), one must have f_D larger than 3. Moreover, all the BLL cores require f_D greater than 1. While this analytical model is oversimplified, it does make it clear that a precise determination of the degree of C and O depletion is necessary if one wishes to estimate $x(e)$. For comparison with the later numerical results, in Table 1 we collate our estimates of the ionization degree and cosmic-ray ionization rate obtained using equations (3) and (4), with $f_D = 2$, 3, and 5. Numbers in boldface represent the best estimate of $x(e)$ and ζ after determining f_D (see § 5).

4. MODEL

We have computed models of the evolution of the chemistry in a dense core [$T = 10$ K, $n(H_2) \sim 10^4 - 10^5\ cm^{-3}$] using a pseudo–time-dependent chemistry code originally developed by Leung, Herbst, & Heubner (1989). Only gas-phase reactions (with the exception of H_2 production and electronic recombination of light ions) are considered, and the chemistry is allowed to evolve from an initial state in which all elements (except hydrogen) are atomic to a final steady state.

We have used the "new standard model" of LBH, which is based on the gas-phase dense cloud model of Herbst & Leung (1989) and includes new elements (Cl and P), a comprehensive sulphur chemistry (Millar & Herbst 1990), and cosmic ray–induced photodestruction reactions. We have further modified the new standard model in order to consider simple deuterated species. In addition, the rate coefficient of the H_3^+ dissociative recombination reaction has been updated to $1.15 \times 10^{-7}(T/300)^{-0.65}$, based on recent laboratory work (M. Larsson 1997, private communication). In Table 2 we list some of the deuteration reactions that we have added to the LBH model.

Although we have studied the evolution of the gas-phase abundances as a function of time, in the subsequent analysis we in general use the steady-state abundances in order to infer the ionization degree and other parameters of the BLL cores. This is partly because the BLL cores are quiescent, and hence we expect their age to be at least one free-fall time, or roughly 10^5 yr for the BLL cores. At this time, R_D and R_H are close to their equilibrium values in most cases (see § 5). In addition, of course, the number of free parameters drastically increases if one is forced to consider so-called early-time chemistry. On the other hand, we note that several of the cores in the BLL sample have large abundances of carbon-chain molecules similar to those observed toward the cyanopolyyne peak in TMC-1. Early-time chemistry has had some success in explaining the abundances observed in TMC-1, which, however, as discussed below, may be quite unique.

For deuterated species, we have in general followed the recommendations of Millar et al. (1989), but we have used the more recent rates given by Larsson et al. (1996) for the dissociative recombination of H_2D^+. These play a critical role in our model because they influence the degree of deuterium fractionation of H_3^+ and thus of HCO^+. Since we focus on the $[DCO^+]/[HCO^+]$ ratio, we neglect other deuterium enrichment reactions, such as

$N + CHD \rightarrow DCN + H$, which are important, for example, when considering the [DCN]/[HCN] ratio (see, e.g., Millar et al. 1989).

The adopted abundances for several key elements critically affect the deuterium fractionation and the ionization degree in our models. Particularly important is the deuterium abundance, which we have taken as 1.5×10^{-5}, consistent with recent determinations of the interstellar value (Linsky et al. 1995; Federman et al. 1996). As in our analytical approach, we assume that the depletions of carbon and oxygen are equal to one another and that they can be described by the depletion factor f_D. There is good evidence that a large fraction of both C and O is in the solid form in dense regions (e.g., Chiar et al. 1995), and one aim of our models is to provide better limits on the fraction remaining in the gas phase. Given the uncertainty in f_D, we have treated it as a free parameter in the range of 2–5, which we determine where possible for the BLL cores. Our assumption that the degrees of depletion for C and O are equal is critical, and we merely note here that we know of no good evidence that this is not correct in dense clouds. A recent ISO study (Whittet et al. 1996) suggests that the ratio of O to C in the form of volatile ices is larger than the solar abundance ratio. However, the oxygen-containing ices in the cases studied seem to be a relatively small fraction of the total oxygen content (van Dishoeck et al. 1993). Terzieva & Herbst (in preparation) are currently investigating the general question of how the time-dependent chemistry is affected by depletions of carbon and oxygen, both equal and unequal, for all three model networks used by LBH. One preliminary conclusion is that selective depletion of oxygen tends to lengthen the time needed to reach peak early-time abundances in the new standard model.

Refractory metals of low ionization potential, such as Mg and Fe, play an important role in determining the electron abundance in dense cores because they can exchange charge with molecular ions, producing Mg^+, Fe^+, etc., which are destroyed relatively slowly by radiative recombination (if, as is customarily assumed, these ions do not themselves react to form molecules). We have used as our standard model the low metal abundance case of LBH. In this case, the elements S, Si, Na, Mg, and Fe are depleted by 2 orders of magnitude relative to typical values in the diffuse interstellar medium (see Table 1 of LBH). This mix has led to good agreement with observations for sulfur-containing molecules (Prasad & Huntress 1982), for complex molecules (Herbst & Leung 1989), and for the ionization balance (e.g., Graedel, Langer, & Frerking 1982). Relative to these standard values, we have varied the abundance of Mg, Na, and Fe between 0.01 and 30 times the standard value. At the low end of this range, the major ion is typically HCO^+, and further depletion becomes irrelevant to the determination of the ionization degree.

5. RESULTS

The main parameters of our standard model are summarized in Table 3. The high value for the visual extinction is merely a device to ensure that photoprocesses are unimportant. Carbon and oxygen abundances are expressed as a function of the depletion factor f_D introduced in § 3. Models with $f_D = 2$, 3, and 5 are labeled "d2", "d3", and "d5", respectively. The models have been run for 10^8 yr in order to achieve a steady-state condition for all species. Before describing our detailed analysis of $x(e)$, we note that a lower (often severely low) limit to this parameter is given by the HCO^+ abundances shown in Figure 1.

TABLE 3

MAIN PARAMETERS OF CHEMICAL MODELS

Parameter	Value
n_H (cm^{-3}).....	2×10^4, 2×10^5
T (K)	10
A_V (mag)	500
ζ (s^{-1})	1.3×10^{-17}
Initial fractional abundances with respect to total hydrogen[a]	
H_2.....	0.5
HD.....	1.5×10^{-5}
C^+	$7.30 \times 10^{-5}/f_D$
O.....	$1.76 \times 10^{-4}/f_D$

NOTE—Total hydrogen density is $n_H = n(H) + 2n(H_2)$; T is the gas kinetic temperature; A_V is the visual extinction; ζ is the cosmic-ray ionization rate.

[a] Initial fractional abundances of He, N, S^+, Si^+, Fe^+, Na^+, Mg^+, P^+, and Cl^+ are as in Table 1 of LBH. The term f_D (=2, 3, and 5) is the depletion factor introduced in § 3.

In Figure 2, the variation of the calculated steady-state electron to HCO^+ abundance ratio in d2 models is plotted against the summed abundance of refractory metals ($M_i^+ \equiv Mg^+$, Fe^+, and Na^+) for different values of the gas density and cosmic-ray ionization rate. At the standard value of $\zeta = 1.3 \times 10^{-17}$ s^{-1}, $[e]/[HCO^+]$ varies between 2 and 10^3 for $\sum_i x(M_i^+) = 10^{-10}$ and 10^{-7}, respectively. The "standard" value of metal abundance is 1.2×10^{-8} (Fig. 2,

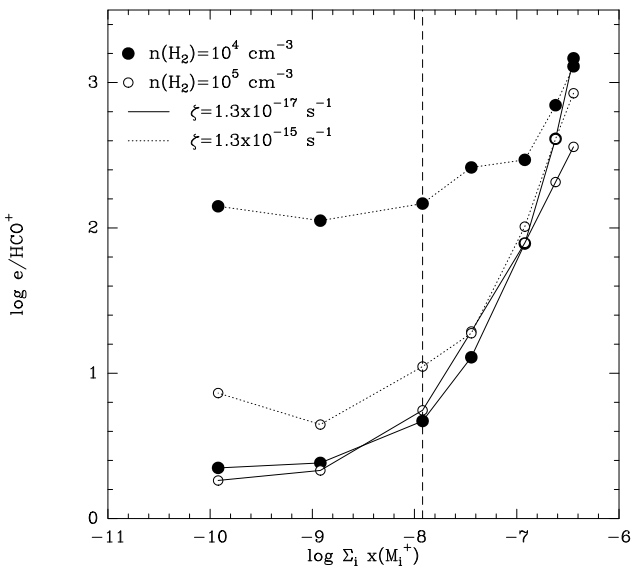

FIG. 2.—The electron to HCO^+ abundance ratio vs. metal abundance $[\sum_i x(M_i^+) = x(Mg^+) + x(Fe^+) + x(Na^+)]$ for d2 models with $n(H_2) = 10^4$ cm^{-3} (*solid circles*) and 10^5 cm^{-3} (*open circles*). Model results for which standard values of ζ ($=1.3 \times 10^{-17}$ s^{-1}) have been used are connected by solid lines, while models with $\zeta = 1.3 \times 10^{-15}$ s^{-1} are connected by dotted lines. The vertical dashed line marks the standard value of metal abundance $[\sum_i x(M_i^+) = 1.2 \times 10^{-8}]$ that corresponds to the so-called low metal abundances (see LBH). At the standard values of ζ and metal abundance, $[e]/[HCO^+] \sim 5$.

dashed line). Assuming standard values of ζ and metal abundances, we expect $[e]/[HCO^+] \sim 5$ for gas densities of $n(H_2) = 10^4$–10^5 cm^{-3}. Note the strong dependence of $[e]/[HCO^+]$ on the cosmic-ray ionization rate at $n(H_2) = 10^4$ cm^{-3}. Similar results are found for d3 models.

In Figure 3, we show the evolution of R_D and R_H as a function of time in d2 models for gas densities $n_H = 2 \times 10^4$ and 2×10^5 cm^{-3}. One sees that both parameters reach steady-state values after at most 3×10^5 years (on the order of the dynamical timescale for the BLL objects).

In order to study the variation of the degree of ionization as a function of a variety of parameters, we have run a set of models with differing cosmic-ray ionization rates, refractory metal abundances, densities, and f_D. In Figure 4, we show our d2 steady-state results for R_H and R_D for cosmic-ray ionization rates between 10^{-19} and 10^{-15} s^{-1} and refractory metal abundances (Mg, Fe, Na) varying between 0.01 and 30 times the standard (LBH) value. The results for observed cores from BLL are shown for comparison. We see that the observations of the BLL sample can reasonably be explained by variation of the cosmic-ray rate and refractory metal abundance by factors of 10 around the standard value, in particular for models with $n_H = 2 \times 10^4$ cm^{-3} (see Fig. 4*a*). This is not, of course, proof that the observed dispersion in R_H and R_D is due to variation in these quantities, but it is consistent with that hypothesis. We will for the moment assume it to be true and consider the consequences. We also, as mentioned in § 2, considered variations of visual extinction to explain the observed R_H and R_D ratios. However, variations of metal depletion and visual extinction do not allow a coverage of the whole range of R_D and R_H values observed by BLL. In fact, for $A_V > 3$ mag, photoprocesses become inefficient, and there are no significant distinctions between models with different A_V.

5.1. *Derived Electron Fractions and Cosmic-Ray Ionization Rates*

For each model depicted by solid circles in Figure 4, the electron fraction and the cosmic-ray ionization rate are known. This allows us to derive contours for $x(e)$ and ζ on a log R_D- log R_H plot. These are given in Figure 5 for d2 models at steady state with $n_H = 2 \times 10^4$ cm^{-3}. The use of contour-level diagrams such as those in Figure 5 allows a direct measurement of the electron fraction and the cosmic-ray ionization rate once R_H and R_D are known from observations. General expressions for the calculation of $x(e)$ and ζ have been found by using a least-squares method to model calculated data points in Figure 4:

$$\log x(e) = a_1 + \frac{a_2}{(\log R_D)^2} + \frac{a_3}{\log R_H} \quad (5)$$

$$\log \zeta = b_1 + \frac{b_2}{\log R_D} + \frac{b_3}{\log R_H} . \quad (6)$$

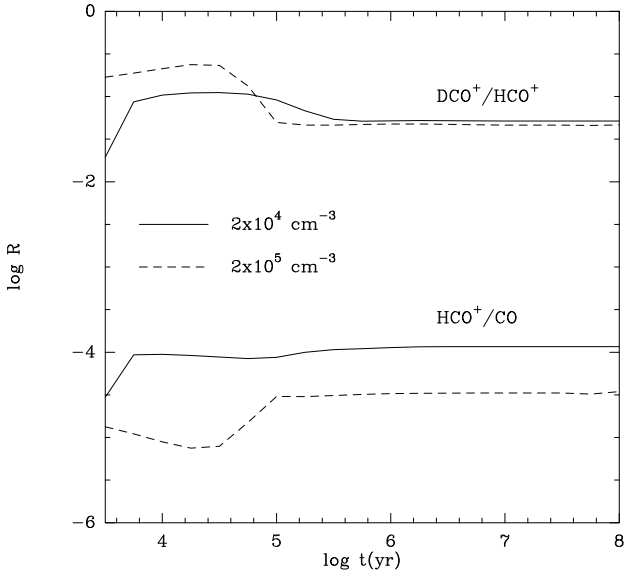

FIG. 3.—Time evolution of the abundance ratios R_D and R_H in d2 models. Note the small dependence of R_D on gas density at steady state.

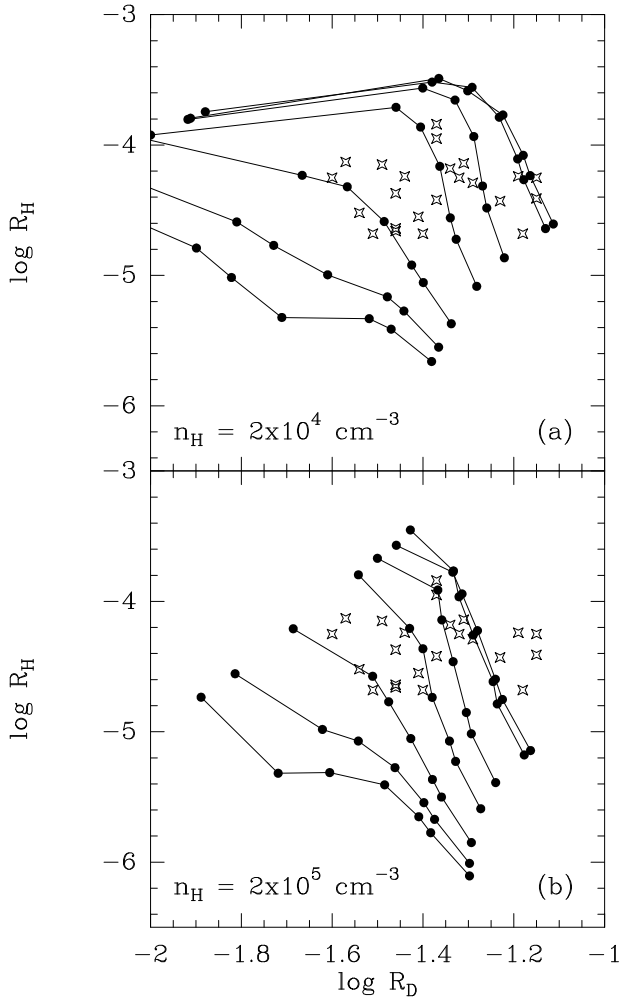

FIG. 4.—R_H as a function of R_D in BLL cores (*stars*) and gas-phase chemical model results at steady state (*solid circles*), where refractory element depletion and cosmic-ray ionization rates have been varied but the C and O depletion is fixed at $f_D = 2$. (*a*) Models with $n_H = 2 \times 10^4$ cm^{-3}; (*b*) models with $n_H = 2 \times 10^5$ cm^{-3}. Continuous lines connect models with the same amounts of metal depletion (from top right to bottom left, the metal abundance is 0.01, 0.1, 1, 3, 10, 20, and 30 times the standard value of 1.2×10^{-8}). Data points on each curve have different values of the cosmic-ray ionization rate: 2.6×10^{-19}, 1.3×10^{-18}, 2.6×10^{-18}, 1.3×10^{-17}, 5.3×10^{-17}, 1.3×10^{-16}, and 1.3×10^{-15} s^{-1}. The smallest value of ζ is at the bottom right of the curves, while the highest value is at the top left. The observed dispersion in R_H and R_D may be explained by variations of ζ and metal abundances by factors of 10 with respect to the standard values.

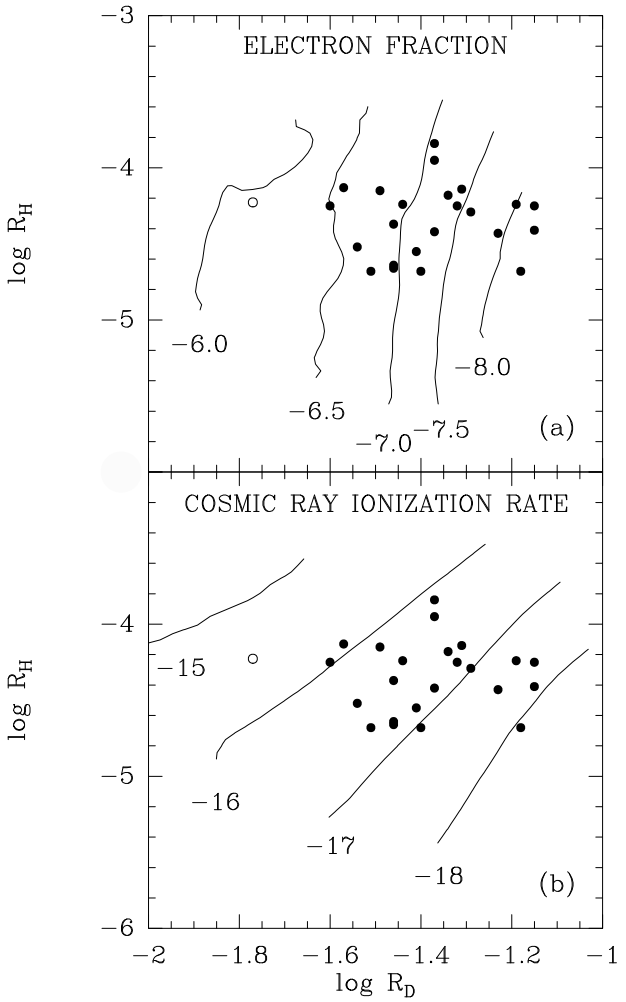

FIG. 5.—Logarithmic contour level diagrams for d2 models of (*a*) electron fraction and (*b*) cosmic-ray ionization rate. The contours have been drawn by using model data points from Fig. 4*a*. The open circle represents TMC-1 (CP) (see Fig. 1). Values of $x(e)$ and ζ can be directly determined with the help of the above diagrams once R_H and R_D are known from observations.

For the refractory metal abundance, we can use a similar approach, which leads to

$$\log \sum_i x(M_i^+) = c_1 + \frac{c_2}{(\log R_D)^2} + \frac{c_3}{\log R_H} . \qquad (7)$$

Tables 4, 5, and 6 list values of the above parameters and corresponding errors for models with $n(H_2) = 10^4$ and 10^5 cm^{-3}, at steady state. Values of a_i, b_i, and c_i ($i = 1, 3$) for models with C and O initially depleted by a factor of 3 and 5 ($f_D = 3$ and 5) are also given in Tables 4, 5, and 6.

Electron fractions, cosmic-ray ionization rates, and metal abundances for BLL's cores calculated with equations (5), (6), and (7) are listed in Table 7, together with gas number densities $n(H_2)$ determined by BLL from their DCO^+ observations. To find $x(e)_p$, ζ_p, and M_p^+ [$\equiv \sum_i x(M_i^+)$] at the corresponding gas density $n(H_2) = 10^p$ cm^{-3} for each core we used the interpolation procedure

$$x(e)_p = 10^{\alpha(4-p)} x(e)_4$$
$$\zeta_p = 10^{\beta(4-p)} \zeta_4$$
$$M_p^+ = 10^{\gamma(4-p)} M_4^+ ,$$

TABLE 4

FIT PARAMETERS FOR $x(e)$

$n(H_2)$ (cm^{-3})	a_1	a_2	a_3	χ_a^2
		$f_D = 2$		
10^4.....	-5.72 ± 0.11	-4.65 ± 0.09	-4.34 ± 0.46	0.48
10^5.....	-4.52 ± 0.14	-7.07 ± 0.16	-3.25 ± 0.48	0.54
		$f_D = 3$		
10^4.....	-5.95 ± 0.11	-3.20 ± 0.06	-3.54 ± 0.42	0.45
10^5.....	-5.14 ± 0.12	-4.71 ± 0.09	-2.92 ± 0.43	0.46
		$f_D = 5$		
10^4.....	-6.27 ± 0.10	-2.03 ± 0.04	-3.24 ± 0.41	0.49
10^5.....	-5.78 ± 0.10	-2.87 ± 0.06	-2.91 ± 0.39	0.48

where $\alpha \equiv \log [x(e)_4/x(e)_5]$, $\beta \equiv \log (\zeta_4/\zeta_5)$, and $\gamma \equiv \log (M_4^+/M_5^+)$. For d2 models, the values of α and β averaged over the whole core sample are 0.37 ± 0.26 and -0.62 ± 0.24, respectively. Within the errors, the above values are consistent with the relation $\alpha \propto (\beta + 1)/2$, valid in the simple model of electron balance in molecular clouds where ions are produced by cosmic rays and destroyed by dissociative recombination. The errors for the interpolated $x(e)$ and ζ values have been found by linearly interpolating $\sigma_{x(e)}$ and σ_ζ at 10^4 and 10^5 cm^{-3}.

One sees from Table 7 that the inferred ionization fractions are extremely sensitive to our assumptions about C/O

TABLE 5

FIT PARAMETERS FOR ζ

$n(H_2)$ (cm^{-3})	b_1	b_2	b_3	χ_b^2
		$f_D = 2$		
10^4.....	-17.08 ± 0.18	7.64 ± 0.15	-23.92 ± 0.57	0.74
10^5.....	-14.12 ± 0.19	10.96 ± 0.21	-24.36 ± 0.46	0.49
		$f_D = 3$		
10^4.....	-17.73 ± 0.17	5.82 ± 0.13	-22.21 ± 0.57	0.85
10^5.....	-15.30 ± 0.15	8.27 ± 0.14	-23.06 ± 0.43	0.45
		$f_D = 5$		
10^4.....	-18.45 ± 0.17	4.17 ± 0.10	-20.79 ± 0.60	1.04
10^5.....	-16.00 ± 0.38	6.06 ± 0.30	-20.32 ± 1.14	4.03

TABLE 6

FIT PARAMETERS FOR $\sum_i x(M_i^+)$

$n(H_2)$ (cm^{-3})	c_1	c_2	c_3	χ_c^2
		$f_D = 2$		
10^4.....	-0.28 ± 0.73	-4.21 ± 0.58	23.30 ± 2.90	19.2
10^5.....	1.92 ± 0.68	-8.23 ± 0.75	25.0 ± 2.35	12.6
		$f_D = 3$		
10^4.....	-0.57 ± 0.64	-3.00 ± 0.38	22.76 ± 2.53	16.4
10^5.....	0.71 ± 0.61	-5.04 ± 0.49	23.90 ± 2.24	12.7
		$f_D = 5$		
10^4.....	-1.16 ± 0.60	-1.86 ± 0.24	21.28 ± 2.37	16.32
10^5.....	-0.32 ± 0.52	-2.92 ± 0.30	21.94 ± 1.99	12.24

TABLE 7

LOGARITHMS OF H_2 DENSITIES, ELECTRON FRACTIONS, COSMIC-RAY IONIZATION RATES, AND METAL ABUNDANCE IN BLL CORES

		$f_D = 2$			$f_D = 3$			$f_D = 5$		
CORE	n	x_e	ζ	M^+	x_e	ζ	M^+	x_e	ζ	M^+
B5	5.2	-7.0 ± 0.2	-16.0 ± 0.3	-7.0 ± 0.9	**-6.6 ± 0.2**	**-15.7 ± 0.2**	**-6.6 ± 0.8**	-6.4 ± 0.1	-15.5 ± 0.7	-6.2 ± 0.6
L1489	5.0	-7.9 ± 0.2	-16.6 ± 0.3	-8.9 ± 1.0	-7.2 ± 0.2	-16.0 ± 0.2	-8.0 ± 0.9	**-6.8 ± 0.1**	**-15.7 ± 0.5**	**-7.3 ± 0.7**
L1495	5.3	-7.5 ± 0.2	-16.5 ± 0.3	-7.7 ± 0.9	**-7.0 ± 0.2**	**-16.0 ± 0.2**	**-7.0 ± 0.8**	-6.6 ± 0.1	-15.7 ± 0.8	-6.5 ± 0.6
L1551–IR	5.2	-9.1 ± 0.2	-18.2 ± 0.3	-9.5 ± 1.0	**-8.0 ± 0.2**	**-17.3 ± 0.2**	**-8.1 ± 0.8**	-7.3 ± 0.1	-16.6 ± 0.7	-7.1 ± 0.6
L43	5.1	-7.9 ± 0.2	-16.6 ± 0.3	-8.7 ± 1.0	**-7.2 ± 0.2**	**-16.1 ± 0.2**	**-7.8 ± 0.8**	-6.8 ± 0.1	-15.7 ± 0.6	-7.2 ± 0.7
B335	5.2	-7.2 ± 0.2	-16.2 ± 0.3	-7.3 ± 0.9	**-6.7 ± 0.2**	**-15.8 ± 0.2**	**-6.8 ± 0.8**	-6.5 ± 0.1	-15.6 ± 0.7	-6.4 ± 0.6
L1174	4.6[a]	-6.9 ± 0.2	-15.9 ± 0.3	-7.8 ± 1.0	**-6.6 ± 0.2**	**-15.7 ± 0.2**	**-7.4 ± 0.9**	-6.4 ± 0.1	-15.6 ± 0.3	-7.0 ± 0.8
L1172	5.2	-6.5 ± 0.2	-15.0 ± 0.3	-7.1 ± 0.9	-6.3 ± 0.2	-14.8 ± 0.2	-6.8 ± 0.8	**-6.2 ± 0.1**	**-14.8 ± 0.7**	**-6.6 ± 0.6**
L1262	5.6	-9.7 ± 0.4	-18.0 ± 0.4	-10.7 ± 0.9	-8.3 ± 0.2	-17.0 ± 0.1	-8.8 ± 0.8	-7.4 ± 0.1	-16.2 ± 1.5	-7.6 ± 0.4
B217	5.4	-8.2 ± 0.3	-16.7 ± 0.3	-9.1 ± 0.9	-7.4 ± 0.2	-16.0 ± 0.2	-8.0 ± 0.8	-6.9 ± 0.1	-15.6 ± 1.0	-7.2 ± 0.5
TMC-2A	4.7[a]	-8.5 ± 0.2	-17.7 ± 0.3	-9.5 ± 1.1	**-7.7 ± 0.2**	**-17.0 ± 0.2**	**-8.4 ± 0.9**	-7.1 ± 0.1	-16.5 ± 0.4	-7.5 ± 0.8
L1536	4.8	-8.3 ± 0.2	-17.6 ± 0.3	-9.0 ± 1.0	**-7.5 ± 0.2**	**-16.9 ± 0.2**	**-8.0 ± 0.9**	-7.0 ± 0.1	-16.5 ± 0.4	-7.2 ± 0.8
TMC-1C	4.4	-6.8 ± 0.2	-16.4 ± 0.2	-7.2 ± 1.0	-6.5 ± 0.2	-16.2 ± 0.2	-6.8 ± 0.9	**-6.4 ± 0.1**	**-16.1 ± 0.3**	**-6.6 ± 0.8**
L234A	4.7	-7.3 ± 0.2	-16.0 ± 0.3	-8.9 ± 1.1	-6.8 ± 0.2	-15.6 ± 0.2	-8.2 ± 0.9	**-6.5 ± 0.2**	**-15.4 ± 0.4**	**-7.6 ± 0.8**
L234E	5.0	-7.2 ± 0.2	-16.0 ± 0.3	-8.0 ± 1.0	**-6.7 ± 0.2**	**-15.6 ± 0.2**	**-7.4 ± 0.8**	-6.5 ± 0.1	-15.4 ± 0.5	-6.9 ± 0.7
L1498	5.0	-7.1 ± 0.2	-16.1 ± 0.3	-7.7 ± 0.9	-6.7 ± 0.2	-15.7 ± 0.2	-7.1 ± 0.8	**-6.5 ± 0.1**	**-15.5 ± 0.5**	**-6.7 ± 0.7**
L1400G	4.0	-7.3 ± 0.2	-17.1 ± 0.3	-8.2 ± 1.1	-6.9 ± 0.2	-16.8 ± 0.2	-7.7 ± 0.9	-6.6 ± 0.1	-16.6 ± 0.2	-7.3 ± 0.8
TMC-2	4.7	-7.5 ± 0.2	-16.8 ± 0.3	-8.0 ± 1.0	-7.0 ± 0.2	-16.4 ± 0.2	-7.4 ± 0.9	**-6.6 ± 0.1**	**-16.1 ± 0.4**	**-6.9 ± 0.8**
TMC-1	5.2	-6.6 ± 0.2	-15.0 ± 0.3	-7.4 ± 0.9	-6.3 ± 0.2	-14.8 ± 0.2	-7.1 ± 0.8	**-6.2 ± 0.1**	**-14.7 ± 0.7**	**-6.8 ± 0.6**
L134A	5.1[a]	-7.2 ± 0.2	-16.3 ± 0.3	-7.3 ± 0.9	**-6.7 ± 0.2**	**-15.9 ± 0.2**	**-6.8 ± 0.8**	-6.5 ± 0.1	-15.7 ± 0.6	-6.4 ± 0.7
L183	4.2	-7.2 ± 0.2	-17.1 ± 0.2	-7.6 ± 1.0	-6.8 ± 0.2	-16.8 ± 0.2	-7.1 ± 0.9	**-6.6 ± 0.1**	**-16.6 ± 0.2**	**-6.7 ± 0.8**
L1696A	4.8	-7.4 ± 0.2	-16.1 ± 0.3	-8.7 ± 1.0	-6.9 ± 0.2	-15.7 ± 0.2	-8.0 ± 0.9	-6.6 ± 0.1	-15.5 ± 0.4	-7.5 ± 0.8
L63	4.8	-8.9 ± 0.2	-18.0 ± 0.3	-9.9 ± 1.1	**-7.9 ± 0.2**	**-17.2 ± 0.2**	**-8.6 ± 0.9**	-7.2 ± 0.1	-16.6 ± 0.4	-7.7 ± 0.8
TMC-1 (CP)	4.9	-6.0 ± 0.2	-14.7 ± 0.3	-6.7 ± 0.9	-6.0 ± 0.2	-14.7 ± 0.2	-6.6 ± 0.8	**-6.0 ± 0.1**	**-14.8 ± 0.4**	**-6.5 ± 0.7**

NOTE—Numbers in boldface indicate our best estimates for each source based on HC_3N/CO data.

[a] In L1174, TMC-2A, and L134A the large velocity gradient (LVG) χ^2 routine used by BLL to find densities did not converge; in these cases we assumed the density derived from NH_3 observations of Benson & Myers (1989).

depletion. In fact, there is typically a factor of 3 difference between our estimates for models d2 and d3. In cases with a low electron fraction (e.g., L1551–IR and L1262), the difference may be more than an order of magnitude. In the same fashion, the inferred cosmic-ray ionization rates have an uncertainty that ranges between 0.5 dex (at high rates) and 1 dex (for low ζ). Despite the variations within individual sources caused by the unknown depletions, there are large variations in $x(e)$ (between $\sim 10^{-8}$ and $\sim 10^{-6}$) and ζ (between $\sim 10^{-18}$ s^{-1} and $\sim 10^{-16}$ s^{-1}) from source to source. We believe that these differences are real and are not simply a reflection of the uncertainties in both the model and in parameters such as C/O depletion (see § 5.2 below). Thus, we conclude that there are real variations in the cosmic-ray flux from core to core, causing corresponding variations in the ionization degree and other parameters.

5.2. *Depletion of Initial* C *and* O *Elemental Abundances*

The preceding discussion has underlined the conclusion that a reliable estimate of the degree of C and O depletion is needed in order to estimate $x(e)$. One approach to this is to study the predictions of our models for species other than DCO^+ and HCO^+ and to compare these with observations where available. With this in mind, we have collated data from the literature on HC_3N (Suzuki et al. 1992; Fuller & Myers 1993; Howe et al. 1994), CCS (Suzuki et al. 1992), C_3H_2 (Bell et al. 1988; Cox, Walmsley, & Güsten 1989; Benson, Caselli, & Myers, in preparation), and NH_3 (Benson & Myers 1989; Suzuki et al. 1992) for the BLL cores and compared the predictions of our steady-state models with the observations. In general, the steady-state fractional abundances of complex molecules (especially with respect to CO) *increase* with increasing f_D, because intermediate ions have less tendency to undergo destructive reactions with O. This paradoxical behavior has already been noted for HC_3N (Ruffle et al. 1997; see also Hartquist, Williams, & Caselli 1996; Millar & Herbst 1990).

The results of this comparison are shown in Figure 6. The column density ratios $N(i)/N(\mathrm{CO})$ ($i \equiv HC_3N$, CCS, C_3H_2, and NH_3) are displayed as a function of R_D in order to allow a direct comparison of the observations with our models. For clarity, only d2, d3, and d5 models with $n(H_2) = 10^4$ cm^{-3} and $\zeta = 1.3 \times 10^{-17}$ and 1.3×10^{-16} s^{-1} are shown in Figure 6. We find a strong dependence of the model $[HC_3N]/[CO]$ abundance ratio on f_D, (i.e., on the depletion of carbon and oxygen). This suggests that it may be possible to use the cyanoacetylene abundance as a measure of the degree of depletion. It is important in this regard that the model $[HC_3N]/[CO]$ ratio seems to be relatively independent of the cosmic-ray ionization rate and refractory metal abundance. A variation of 10 in the cosmic-ray ionization rate causes a change in the predicted $[HC_3N]/[CO]$ ratio by a factor of <2. Depletion of N, together with C and O, does not change the results shown in Figure 6; the steady-state $[HC_3N]/[CO]$ ratio still increases by 1 order of magnitude if the three elements are initially depleted by a factor of 5. We therefore conclude from Figure 6 that f_D in the BLL cores varies between 2 and 5. We note that this is consistent with the conclusion of Lemme et al. (1995) for L1498, who found that $[C^{18}O]/[H_2]$ is depleted by a factor of 3 relative to the "canonical" Frerking, Langer, & Wilson (1982) value.

Although we conclude that $[HC_3N]/[CO]$ is a useful depletion estimator in cold cores, we note that the observational data show trends that we do not entirely understand. In particular, we show in Figure 7 a plot of the observed abundance ratios of $[HC_3N]/[C_3H_2]$ against R_D. This shows a surprisingly good correlation in the sense that

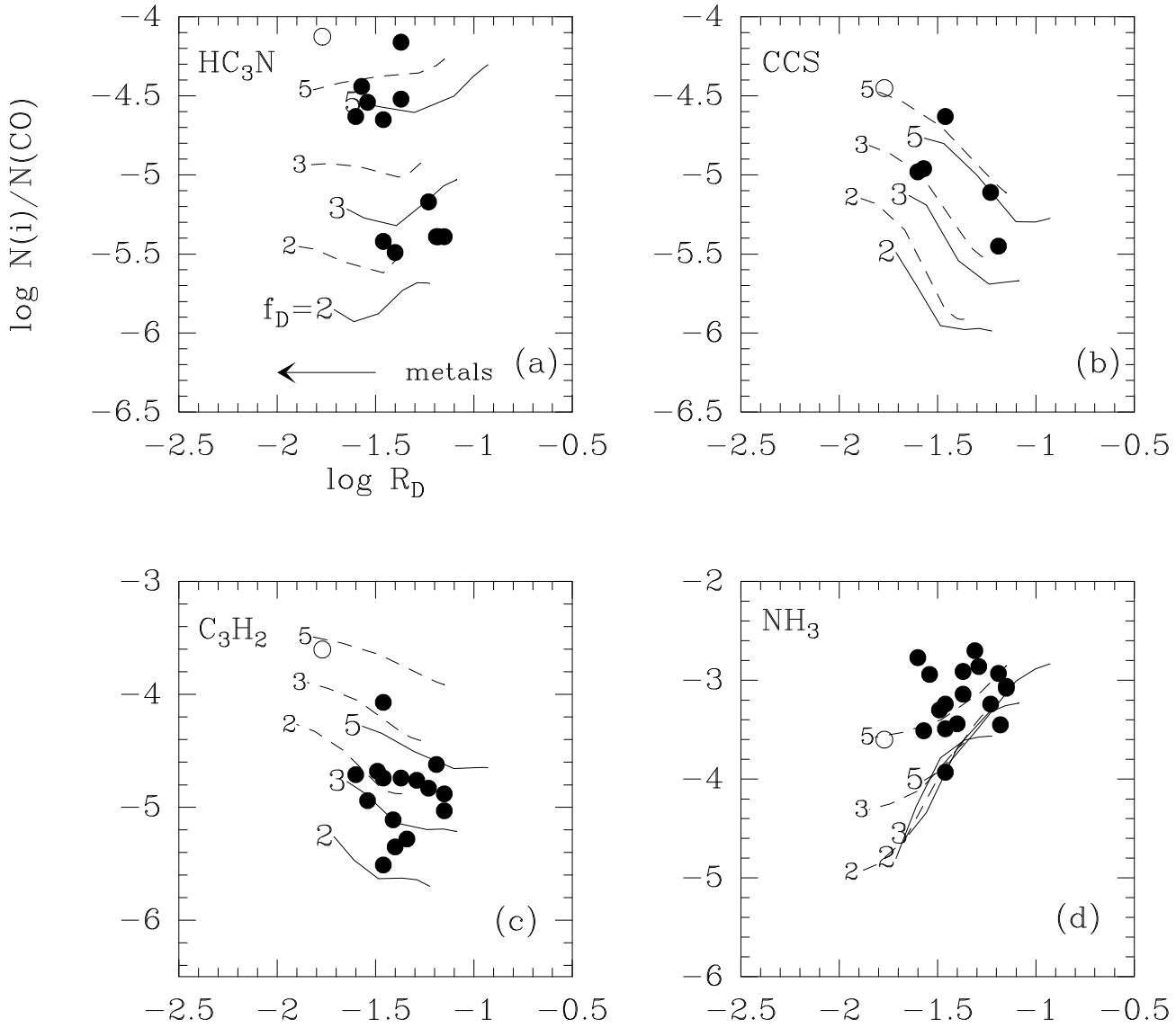

FIG. 6.—(*a*) Cyanoacetylene to CO abundance ratio as a function of R_D predicted by the models, compared with observed values in BLL cores (*solid circles*). The model predictions are for depletion factors $f_D = 2$, 3, and 5 and for cosmic-ray ionization rates of $\zeta = 1.3 \times 10^{-17}$ s^{-1} (*thin curves*) and 1.3×10^{-16} s^{-1} (*dashed curves*). (*b*) Same as (*a*), for CCS. (*c*) Same as (*a*), for C_3H_2. (*d*) Same as (*a*), for NH_3. Note that TMC-1 (CP) (*open circle*) has the highest HC_3N, CCS, and C_3H_2 fractional abundances.

$[HC_3N]/[C_3H_2]$ decreases with increasing R_D, and we conclude that $[HC_3N]/[C_3H_2]$ may for unknown reasons depend upon the ionization degree. The model results give no clear explanation for this, suggesting that there are secrets in the chemistry yet to be uncovered.

The models do suggest that the other abundance ratios do not allow as good an estimate of depletion as $[HC_3N]/[CO]$ because other parameters affect those ratios. In particular, the CCS fractional abundance increases with the abundance of the refractory metals (Fig. 6*b*), while C_3H_2 is very sensitive to the cosmic-ray flux (Fig. 6*c*). The case of ammonia differs from carbon-bearing molecules. In fact, from Figure 6*d* it is evident that the C and O abundances do not affect the $N(NH_3)/N(CO)$ ratio strongly.

Figure 6 also shows that TMC-1 (CP) has a higher HC_3N (and CCS and C_3H_2) abundance than all the other BLL cores. The overabundance of cyanopolyynes (of which HC_3N is the simplest example) in TMC-1 has normally been ascribed to early-time chemistry, whereas the predictions in Figure 6 are based upon our steady-state results. As Ruffle et al. (1997) have pointed out, and as our results also make clear, high C and O depletion is an alternative way of explaining the exceptionally high abundances of C-rich molecules observed in TMC-1. However, as discussed below (§ 7), we consider it more likely that TMC-1's exceptional characteristics are due to its youth.

5.3. *Depletion Estimate*

For some of the cloud cores in our sample, in particular the ones with high R_D values and corresponding low electron fractions (e.g., L1551–IR, L1262, TMC-2A, and L63), a measurement of the depletion factor f_D is crucial for a determination of $x(e)$ (see Table 7). In this section, we will attempt to use the HC_3N data to determine the amount of depletion in the BLL cores.

In Figure 8, a comparison between the $[HC_3N]/[CO]$ observational data and our steady-state models is shown. Models with $n(H_2) = 10^4$ cm^{-3} are shown to the left, those

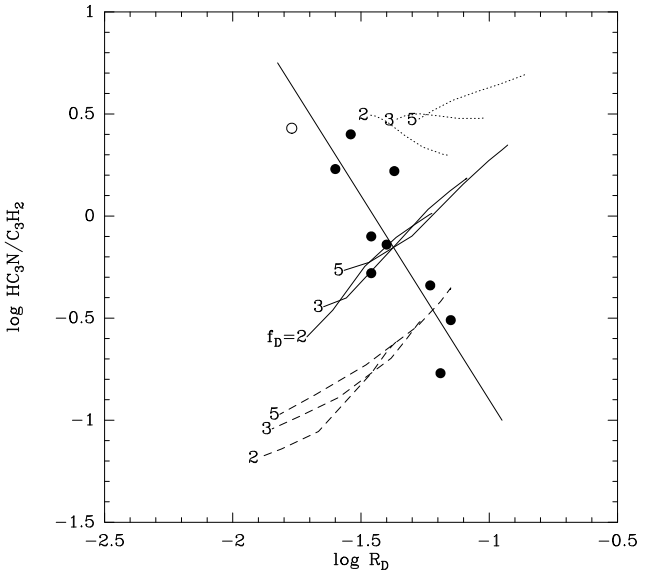

FIG. 7.—Plot of $[HC_3N]/[C_3H_2]$ against R_D. Model results at different values of f_D and ζ are shown: $\zeta = 1.3 \times 10^{-17}$ s^{-1} (*thin curves*), 1.3×10^{-16} s^{-1} (*dashed curves*), and 1.3×10^{-18} s^{-1} (*dotted curves*). The best-fit line is also shown [$\log (HC_3N/C_3H_2) = (-2.9 \pm 0.7) - (2.0 \pm 0.5) \log R_D$; TMC-1 (CP) has not been included in the fit]. The linear correlation coefficient is -0.81. This good correlation cannot be explained with our models by simply varying the metal content, the amount of C and O depletion, and the cosmic-ray ionization rate.

with $n(H_2) = 10^5$ cm^{-3} to the right. The corresponding factor f_D is shown in the top left of each pair of figures. From Figure 8, it is clear that d3 models are appropriate for the group of cores with $[HC_3N]/[CO] < 10^{-5}$ (i.e., B335, L1536, TMC-2A, L63, L1551–IRS, and L1495), whereas d5 models are needed to reproduce observations when $[HC_3N]/[CO] > 10^{-5}$ (i.e., TMC-1, TMC-1C, TMC-2, L1172, and L1498). The two cores with the highest cyanoacetylene abundance, TMC-1 (CP) and L234A, require depletion factors $f_D > 5$.

Estimates of $[HC_3N]/[CO]$ in a few other cores are available, although observed positions are significantly different from those used by BLL during their DCO^+ and $H^{13}CO^+$ survey (for this reason, such cores are not reported in Figs. 6 and 8). For these additional cores, the values of $\log [HC_3N]/[CO]$ are -5.5 in B5N, -4.8 in L1489, -5.4 in L43E (Suzuki et al. 1992), and -4.6 in L183 (Fuller & Myers 1993). Therefore, B5N and L43E may belong to the $f_D = 3$ group of cores, whereas L1489 and L183 probably have C and O depleted by a factor of 5. New observations are needed to confirm the above results.

For the other cores in the sample (L1174, L1262, B217, L234E, L1400G, L134A, and L1696A), no HC_3N observations are available, and hence no f_D estimates can be made. In the case of L1174, L234E, and L134A, this is not a problem for defining $x(e)$ and ζ, which change no more than a factor of 3–5 from d2 to d5 models. Estimates of f_D are, however, very important for the rest of the cores. Note in particular the case of L1262, where $x(e)$ varies by as much as a factor of 200 when f_D changes from 2 to 5 (see Table 7).

Our best estimates of $x(e)$ for each source, based on HC_3N/CO data, are shown boldface in Table 7. These, as well as ζ values, are compared in Figure 9 with $x(e)$ values from the analytical model (see also Table 1). Values of $x(e)$ and ζ for L63 cannot be calculated with the analytical model, perhaps suggesting a poor estimate of f_D in this case. Note that equations (3) and (4) tend to overestimate $x(e)$ and ζ by a factor of a few for intermediate to high values of the ionization degree.

5.4. *Comparison between x(e) and Cloud Core Parameters*

It is also of interest to compare the derived ionization degree with other core parameters. In Figure 10, we show our computed $x(e)$ as a function of $C^{18}O$ (and implicitly hydrogen) column density, H_2 number density, DCO^+ line width, and R_H. The comparison with $C^{18}O$ column density allows a check on whether the external photon field plays a role in determining the ionization degree. If this were the case, one might expect higher $x(e)$ for lower $C^{18}O$ column density and hence lower visual extinction. We see no evidence for this, and so conclude that our assumption that the radiation field may be neglected is justified. No correlation is found between $x(e)$ and $n(H_2)$. Figure 10*b* also reports the relation expected if the electron fraction is due to cosmic-ray ionization alone and ζ has its standard value [$x(e) \sim 1.3 \times 10^{-5} n(H_2)^{-1/2}$; cf. McKee 1989]. The majority of the cores lie above the dashed line, indicating that higher values of cosmic rays (and different metal abundances) must be considered in order to correctly determine $x(e)$.

The comparison between derived $x(e)$ and BLL's observed line widths is of interest because it has been suggested (Charnley & Roberge 1992) that ambipolar diffusion driven by Alfvén waves could drive certain ion-molecule reactions that affect deuterium fractionation. Such effects are neglected by us. We conclude that there is no correlation, based on Figure 10*c*. In contrast, Charnley & Roberge (1992) predict a slight decrease in deuterium fractionation and hence an increase in implied $x(e)$ for large line width. This reflects the relation between the R_D and Δv discussed in § 2. However, more sensitive and more spatially resolved measurements are probably needed to better define the above correlations. Finally, we find that both $x(e)$ and ζ correlate well with R_D but not with R_H (Fig. 10*d*).

6. AMBIPOLAR DIFFUSION VERSUS FREE-FALL TIME

The standard model of low-mass star formation (e.g., Shu et al. 1987) relies on the low ionization degree of molecular clouds in two ways: (1) the density of ionized gas must be high enough for ion-neutral collisions to couple the magnetic field to the neutral gas, thereby providing magnetic field support against gravity, and (2) in a dense core, the density of ionized gas must be low enough to allow neutrals to slip past the ions via ambipolar diffusion and eventually cause gravitational collapse. The level and structure of ionization in molecular clouds is thus a crucial aspect of our understanding of how stars form.

The electron fraction calculated above and the density values derived from DCO^+ observations of BLL allow us to investigate the magnetic stability of low-mass cores against gravitational collapse. To calculate the ambipolar diffusion (t_{AD}) and free-fall (t_{ff}) times, we used equations (13.57) and (13.47), respectively, from Spitzer (1978). The results are shown Table 8 and in Figure 11*a*, where t_{AD} is reported as a function of t_{ff} for low-mass cores in the BLL sample. The errors for t_{AD} reflect the uncertainty in $x(e)$. All the cores have $t_{AD} > t_{ff}$, indicating that magnetic fields and ion-neutral coupling may support them against gravity. Note that there is no difference in the t_{AD}/t_{ff} ratio between cores with embedded stars and starless cores.

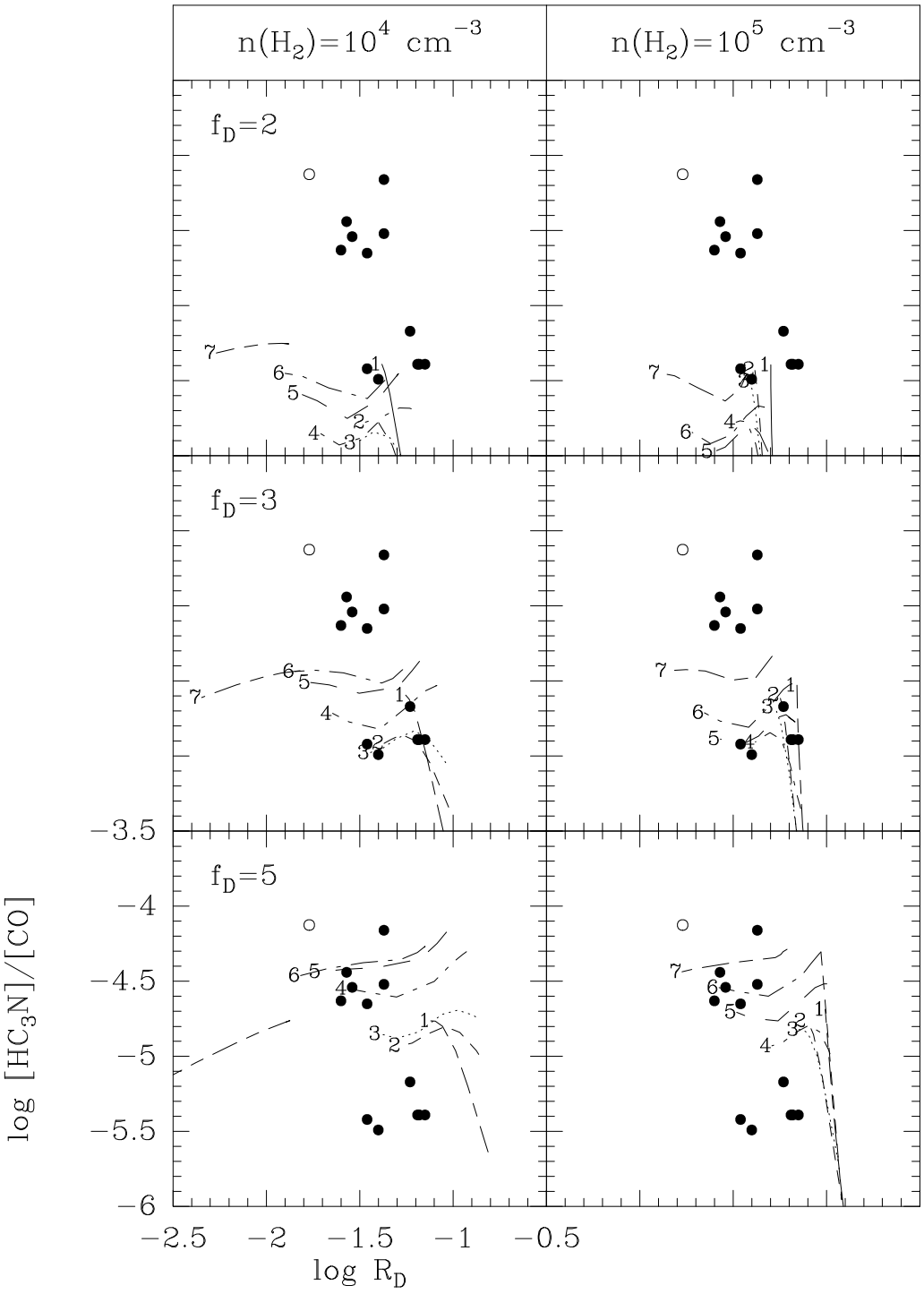

FIG. 8.—Comparison between the observed $[HC_3N]/[CO]$ abundance ratio vs. R_D in BLL cores (see Fig. 6) and chemical models with a different density $n(H_2)$, depletion factor f_D, metal abundances (which increases from right to left), and cosmic-ray ionization rates (each number indicates model results at a fixed value of ζ and different metal abundances; see also Fig. 4). ζ values increase from 2.6×10^{-19} s^{-1} (*curves marked* "1") to 1.3×10^{-15} s^{-1} (*curves marked* "7"). Cores with $[HC_3N]/[CO] < 10^{-5}$ are better explained by models with $f_D = 3$, whereas cores with $[HC_3N]/[CO] > 10^{-5}$ are consistent with $f_D = 5$.

Table 8 (see also Fig. 11*b*) also reports the so-called wave coupling number, or the ratio of the region of size r to the cutoff wavelength for propagation of magnetohydrodynamic (MHD) waves (see eq. [10] of Myers & Khersonsky 1995, hereafter MK). Figure 11*b* shows log W as a function of log $x(e)$. In the calculation of W, a magnetic field value of 10 μG and a gas temperature of 10 K have been assumed. As explained by MK, W is the ratio of maximum to minimum wavelength that can propagate in a region; it can be considered a magnetic Reynolds number for motions associated with MHD waves. When $W \gg 1$, the field and fluid are well coupled for a wide range of wavelengths, which is the case for all the cores in our sample (see Fig. 11*b*).

In Figure 12*a*, we plot the histogram of ambipolar diffusion times t_{AD} for the BLL cores. In Figure 12*b*, we plot the

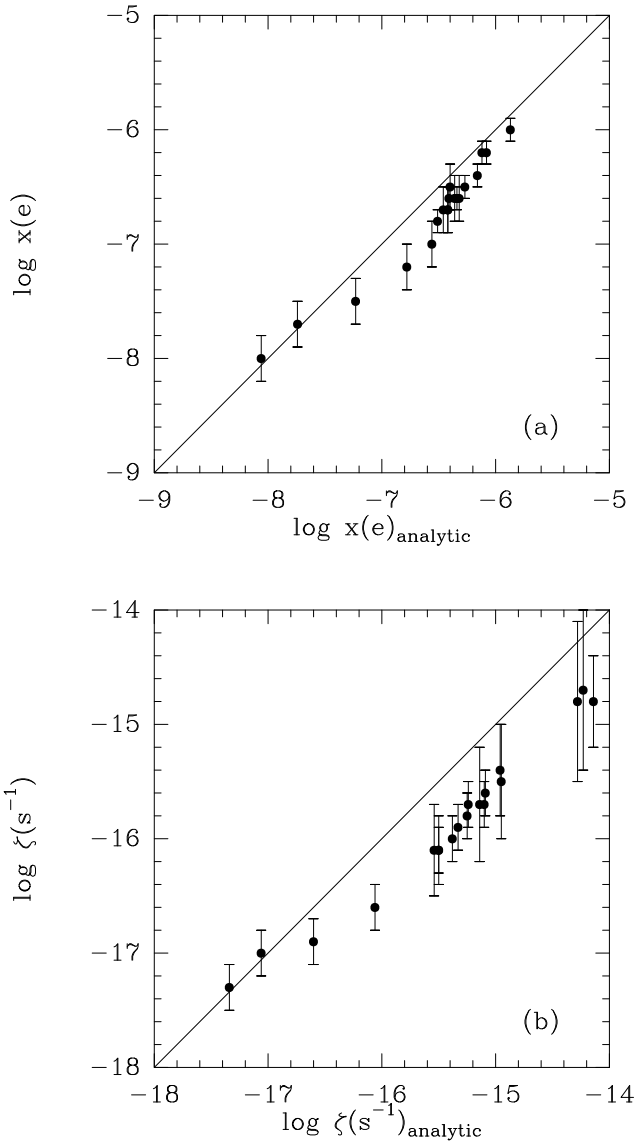

FIG. 9.—(*a*) Electron fraction and (*b*) cosmic-ray ionization rate from numerical models vs. the analytically determined $x(e)$ and ζ. The simpler analytical method slightly overestimates the two quantities when $x(e) > 10^{-7}$ and $\zeta > 10^{-17}$ s^{-1}. The electron fraction and the cosmic-ray ionization rate of the L63 core cannot be analytically determined (see Table 1 and eq. [3]). Values of f_D from § 5.3 have been adopted.

histogram of the ratio t_{AD}/t_{ff} for the same sample. The median t_{AD} is $10^{6.7}$ yr and there are four sources (20%) with $t_{AD} < 10^6$ yr or with $t_{AD}/t_{ff} < 10$. The median core in this sample has $t_{AD}/t_{ff} = 50$, and hence, if their magnetic flux is indeed sufficient to prevent collapse, they will be much longer lived than suggested by their dynamical timescales.

This seems to be in contradiction with the fact that five cores with $t_{AD} \sim 4 \times 10^6$–$10^7$ yr are associated with embedded (Class I) *IRAS* sources whose lifetime is thought to be of the order of 10^5 yr. Naively, one would expect that from a sample of cores with ambipolar diffusion times in this range, only a fraction t_{IRAS}/t_{AD} (where t_{IRAS} is the lifetime for the embedded class I phase) should show evidence of embedded young stars. While the BLL sample is not unbiased, this seems to contradict our results. The explanation of this paradox is unclear. It could perhaps have to do with the origin and evolution of the cosmic-ray flux, which has been considered as a free parameter in our treatment. It could also indicate that ambipolar diffusion is not the fundamental process regulating star formation in nearby dark clouds. However, we caution that, as Table 8 makes clear, our estimates of t_{AD} are still extremely uncertain.

7. THE EXCEPTIONAL CORE TMC-1 (CP)

BLL did not observe the cyanopolyyne peak in TMC-1 where many long-chain carbon molecules have been found (see, e.g., Langer et al. 1997), and thus TMC-1 (CP) does not properly form part of our sample. However, there are reliable measurements of R_D and R_H available for this object (Guélin et al. 1982), and we have therefore included it in much of our analysis. As is clear from Figures 5 and 6, TMC-1 (CP) is exceptional not only for its high abundances of long-chain carbon species but also for the low values of R_D in this object. In terms of our models, this implies a relatively large value of $x(e)$ (see Table 7) and also of the cosmic-ray ionization rate. Indeed, the value given for ζ (2×10^{-15} s^{-1}) in Table 7 is so high that it would imply temperatures higher than are observed; we conclude that the likeliest explanation of the data is that TMC-1 is extremely young and that the steady-state solutions are not valid in this case. In other terms, so-called early-times abundances are the best explanation of both the carbon-rich molecules and the low degree of deuterium enrichment. Thus, a high degree of C and O depletion, as proposed by Ruffle et al. (1997), seems to us an unlikely explanation of TMC-1 (CP)'s peculiar abundance distributions. In any case, our analysis underlines the point that TMC-1 (CP) is peculiar both as far as deuterium fractionation is concerned and with regard to long-chain carbon species. It is thus misleading to use the TMC-1 abundance distribution as typical.

The above discussion makes clear, however, that the assumption of steady-state abundances is likely to lead to errors of lesser degree in other cores as well. For the reasons discussed earlier, we feel that steady state is a reasonable assumption for the majority of objects, but clearly this is not true in all cases.

8. DISCUSSION

The degree of ionization $x(e)$ in dark cores plays a critical role in star formation through its regulation of ambipolar diffusion. In this paper, we have reported how $x(e)$ as well as the cosmic ray ionization rate ζ can be estimated from observational data for 24 dark cores. The method uses observed values of $R_D = [DCO^+]/[HCO^+]$ and $R_H = [HCO^+]/[CO]$ and compares them with steady-state values obtained from detailed pseudo–time-dependent chemical models. Inputs into the models include the elemental abundances as well as the cosmic-ray ionization rate ζ(s^{-1}). Outputs include the fractional ionization $x(e)$ as well as abundances for a wide assortment of atoms and molecules. The calculated electron abundance is strongly dependent on the gas-phase elemental abundances of the ionizable metals and is also dependent, especially for cores with low ionization, on f_D, the degree of depletion of elemental C and O from the "low metal" values used by LBH. The parameter f_D can be determined by comparing observed HC_3N abundances with calculated ones, since in steady state the abundance of HC_3N increases with increasing f_D. We have used this fact to estimate f_D for cores where

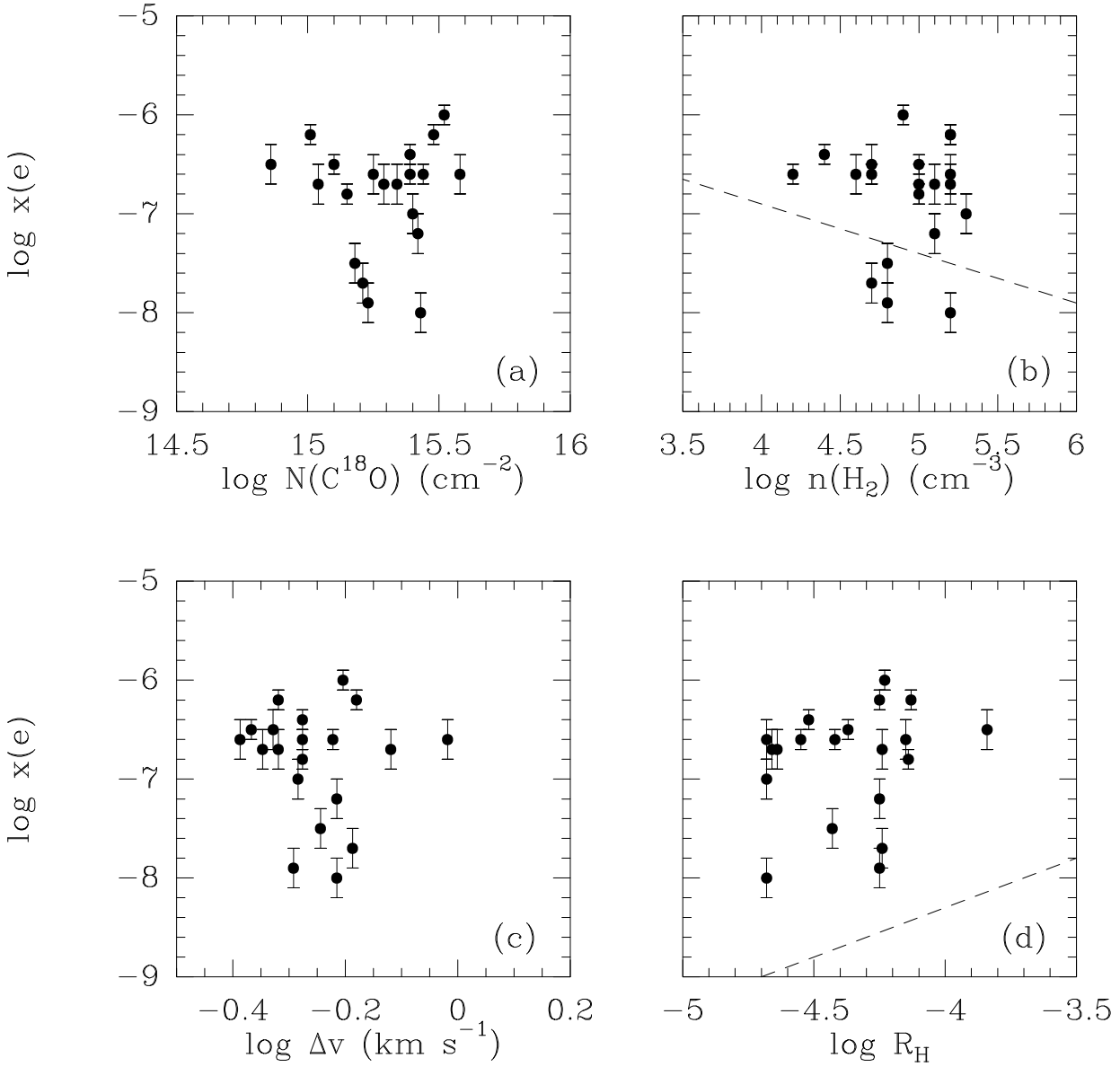

FIG. 10.—Calculated electron fraction for the BLL cores using numerical models as a function of (*a*) $C^{18}O$ column density $N(C^{18}O)$; (*b*) gas number density $n(H_2)$; (*c*) DCO^+ line width Δv; and (*d*) the R_H abundance ratio. The dashed line in (*b*) shows the relation expected if the electron fraction is simply due to cosmic-ray ionization with $\zeta = 1.3 \times 10^{-17}$ s^{-1}. The dashed line in (*d*) represents the lower limit of $x(e) = [HCO^+]/[H_2] = 1.5 \times 10^{-4}/f_D \times [HCO^+]/[CO]$ (here we adopt $f_D = 3$).

HC_3N observations are available, and we have used the f_D values obtained in this fashion to refine our estimates of $x(e)$. We point out that the parameter range (and in particular the abundances for refractory species) studied by us has the consequence that our solutions are not in general affected by conditions of bistability (e.g., Le Bourlot, Pineau des Forêts, & Roueff 1995).

We find that for the cores studied, the fractional ionization ranges from $\sim 10^{-6}$ to 10^{-8}, with ζ in the range of 10^{-16}–10^{-18} s^{-1}. These are large ranges, given the normally assumed homogeneity of the dark cloud cores, but we regard them as real. The range of cosmic-ray ionization rates includes some rather low values ($\zeta < 10^{-18}$ s^{-1}), which imply, from a rather simple estimate of heating and cooling ratios based on Goldsmith & Langer (1978) and Neufeld, Lepp, & Melnick (1995), temperatures below 10 K. One way to overcome this inconsistency is to further deplete carbon and oxygen (see Table 7). On the other hand, the values of ζ derived for TMC-1 (ammonia peak, cyanopolyyne peak) are so high from a thermal standpoint that early-time chemistry must be invoked.

Our estimates of $x(e)$ can be translated into estimates of the ambipolar diffusion timescale t_{AD}. We find that t_{AD} in our sample of cores is typically $\sim 5 \times 10^6$ yr, or roughly 50 times the free-fall time. However, there is a large spread around these values, and there is a minority of cores (20%) for which t_{AD} is only marginally greater than t_{ff}. The dispersion, according to our models, mainly reflects dispersion in the cosmic-ray ionization rate, which would suggest that the cosmic-ray flux is decisive in determining whether a core can collapse to form a star. In this context, it is disturbing that there is no differentiation in our results between cores associated with an embedded *IRAS* source and starless cores. In other words, there is no evidence for a population

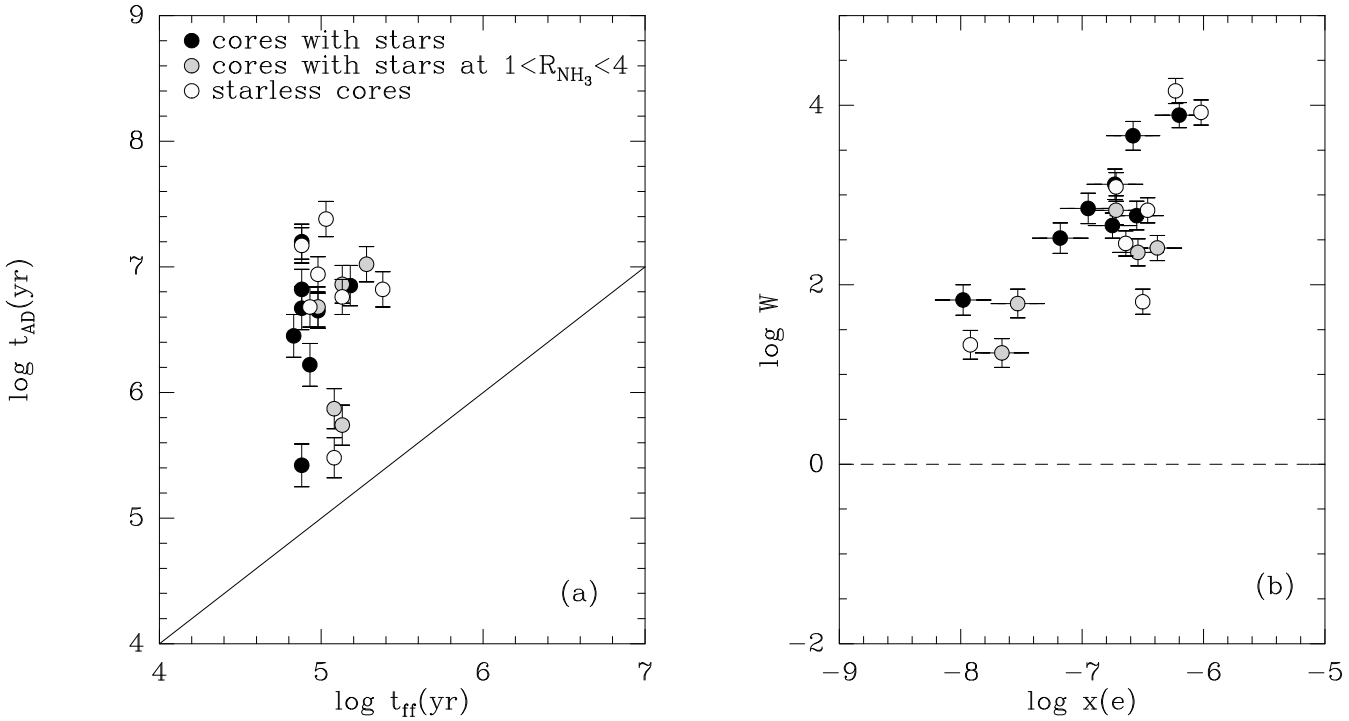

FIG. 11.—(*a*) Ambipolar diffusion (t_{AD}) vs. free-fall (t_{ff}) timescales in low-mass cores. The line marks the region where $t_{AD} = t_{ff}$. All the cores lie above the line, indicating that they are "magnetically stable" against gravitational collapse. (*b*) Wave coupling number W as a function of electron fraction $x(e)$ in low-mass cores. Most of the cores have $W \gg 1$, which suggests a strong ion-neutral coupling. The cores closest to the $W = 1$ line are L1551–IR, L1262, TMC-2A, and L63, which also have the shortest t_{AD}. Solid circles represent cores with stars; shaded circles are cores with stars whose distance from the ammonia core is $1 < R_{NH_3} < 4$ (R_{NH_3} is the radius of the NH_3 half-maximum contour, determined by Benson & Myers 1989); open circles are starless cores. Note that the presence of embedded stars inside the core does not affect its ionization degree and the corresponding values of t_{AD} and W.

TABLE 8

AMBIPOLAR DIFFUSION AND FREE–FALL TIMES IN LOW-MASS CORES

Core	log t_{AD} (yr)	log t_{ff} (yr)	log r (pc)	log W
Cores with stars				
B5	6.8 ± 0.2	4.88	−0.87	3.7
L1489	6.7 ± 0.1	4.98	−1.40	2.7
L1495	6.5 ± 0.2	4.83	−1.46	2.9
L1551–IR	5.4 ± 0.2	4.88	−1.30	1.8
L43	6.2 ± 0.2	4.93	−1.26	2.5
B335	6.7 ± 0.2	4.88	−1.26	3.1
L1174	6.9 ± 0.2	5.18	−0.89	2.8
L1172	7.2 ± 0.1	4.88	−1.02	3.9
Cores with stars at $1 < R_{NH_3}$[a] < 4				
TMC-2A	5.7 ± 0.2	5.13	−1.46	1.2
L1536	5.9 ± 0.2	5.08	−1.19	1.8
TMC-1C	7.0 ± 0.1	5.28	−1.12	2.4
L234A	6.9 ± 0.2	5.13	−1.46	2.4
L234E	6.7 ± 0.2	4.98	−1.26	2.8
Cores without stars				
L1498	6.9 ± 0.1	4.98	−1.52	2.8
TMC-2	6.8 ± 0.1	5.13	−1.26[b]	2.5
TMC-1	7.2 ± 0.1	4.88	−0.72	4.2
L134A	6.7 ± 0.2	4.93	−1.15	3.1
L183	6.8 ± 0.1	5.38	−1.22[b]	1.8
L63	5.5 ± 0.2	5.08	−1.26	1.3
TMC-1 (CP)	7.4 ± 0.1	5.03	−0.72	3.9

[a] R_{NH_3} is the FWHM radius of the ammonia core (from Benson & Myers 1989).

[b] Core size has been estimated from unpublished NH_3 (for TMC-2) and N_2H^+ (for L183) data (Caselli et al., in preparation).

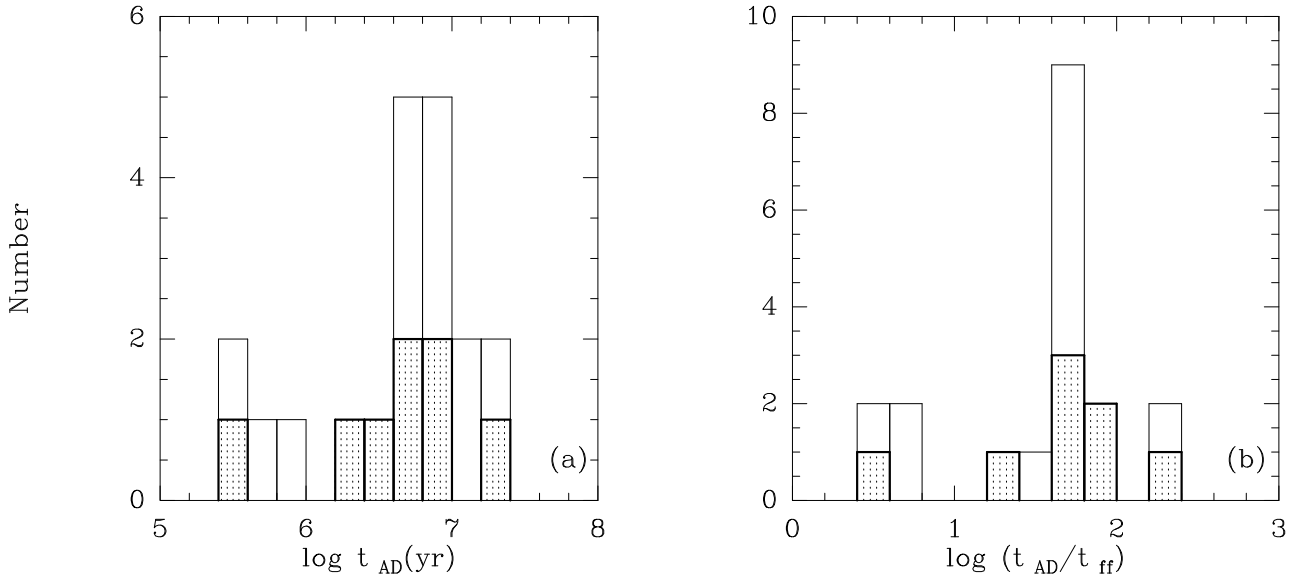

FIG. 12.—(*a*) Histogram of ambipolar diffusion timescales t_{AD} for the BLL cores. (*b*) Histogram of the ratio of the ambipolar diffusion timescales t_{AD} to the free-fall timescale t_{ff}. The shaded columns show the results for cores with embedded *IRAS* sources.

of starless cores with long ($>3 \times 10^6$ yr) ambipolar diffusion times. This may be due to selection effects in our sample, or it may indicate that ambipolar diffusion is not the decisive process regulating star formation in these objects. Alternatively, of course, it may merely reflect the defects in our models of deuterium enrichment in these objects. Certainly, our estimates of $x(e)$ are sufficiently imprecise (see Table 7) that one should be extremely cautious about drawing conclusions from them about the mechanisms of star formation.

It is also clear from our results that an advance in this field will require precise determinations of the degree of depletion of C, N, and O. We have found that for those clouds with observed HC_3N abundances, the elemental carbon and oxygen depletions, f_D (relative to the LBH standard values), are typically in the range of 2–5. These depletions signify that in these "old" cores, $\sim 1/10$ of the cosmic carbon and oxygen still resides in the gas phase, and that desorption is not an efficient process. These depletions partially explain the differences that BLL found between densities derived from DCO^+ and densities based on the $C^{18}O$ column density. One consequence is that masses and column densities based on $C^{18}O$ have been underestimated by factors of order 2. It should be possible to check these statements with measurements of the millimeter emission from the associated dust.

The value of $x(e)$ also depends critically upon the abundance of refractory metals such as Mg and Fe. We have also used our models to estimate the degree of depletion of these species, and we find values between ~ 0.01 (L63) and ~ 10 (B5) times the standard low-metal abundance, $\sum_i x(M_i) = 1.2 \times 10^{-8}$. The metal abundance is a poorly constrained parameter, but the values obtained here corroborate the view of Graedel et al. (1983) that metals are highly depleted in dense cloud cores.

In addition to the use of a detailed chemical model, we have shown that an analytical model based on the work of Wootten et al. (1979), Dalgarno & Lepp (1984), and others is of some utility in determining $x(e)$ and ζ from R_D and R_H, once the amount of C and O depletion is known. High values of R_D (≥ 0.05) cannot be accounted for by the analytical model if $f_D \leq 2$. In these cases, $x(e)$ and ζ calculated with the detailed model also suffer from large uncertainties.

We have utilized steady-state abundances instead of early-time abundances for our analysis. It is well known that large abundances of complex molecules are associated with early times rather than with a steady state, but it is now being appreciated (Ruffle et al. 1997) that reasonable depletions of the elements C and O ($f_D \sim 2$–5) can enhance the steady-state abundances of complex molecules sufficiently to explain the HC_3N abundance in many sources. A steady-state analysis with depletion, however, begs the question of how the gas-phase abundances can be maintained. Either desorption processes are sufficiently efficient to allow at least some C and O to remain in the gas perpetually, or, more likely, our analysis is oversimplified and a more accurate detailed chemical model should include both gas-grain interactions and grain chemistry, in a time-dependent framework. Finally, we note that our steady-state analysis cannot reproduce the complex molecule abundances seen toward TMC-1 (CP), and that this perhaps unique dark core still must be compared with early-time abundances.

P. C. and M. W. acknowledge support from the ASI grant 94-RS-152, ASI grant ARS-96-66, and Consiglio Nazionale delle Richerche (CNR) grant 96/00317. E. H. acknowledges the support of the National Science Foundation for his research program in interstellar chemistry.

REFERENCES

Bell, M. B., Avery, L. W., Matthews, H. E., Feldman, P. A., Watson, J. K. G., Madden, S. C., & Irvine, W. M. 1988, ApJ, 326, 924
Benson, P. J., & Myers, P. C. 1989, ApJS, 71, 89
Bettens, R. P. A., Lee, H.-H., & Herbst, E. 1995, ApJ, 443, 664
Butner, H. M., Lada, E. A., & Loren, R. B. 1995, ApJ, 448, 207 (BLL)
Caselli, P., Hasegawa, T. I., & Herbst, E. 1994, ApJ, 421, 206
Charnley, S. B., & Butner, H. 1995, Ap&SS, 224, 443
Charnley, S. B., & Roberge, W. G. 1992, in Astrochemistry of Cosmic Phenomena, ed. P. D. Singh (Dordrecht: Kluwer), 155
Chiar, J. E., Adamson, A. J., Kerr, T. H., & Whittet, D. C. B. 1995, ApJ, 455, 234
Cox, P., Walmsley, C. M., & Güsten, R. 1989, A&A, 209, 382
Dalgarno, A., & Lepp, S. 1984, ApJ, 287, L47
de Boisanger, C., Helmich, F. P., & van Dishoeck, E. F. 1996, A&A, 310, 315
Federman, S. R., Weber, J., & Lambert, D. L. 1996, ApJ, 463, 181
Frerking, M. A., Langer, W. D., & Wilson, R. W. 1982, ApJ, 262, 590
Fuller, G. A., & Myers, P. C. 1993, ApJ, 418, 273
Goldsmith, P. F., & Langer, W. D. 1978, ApJ, 222, 881
Graedel, T. E., Langer, W. D., & Frerking, M. A. 1982, ApJS, 48, 321
Guélin, M., Langer, W. D., & Wilson, R. W. 1982, A&A, 107, 107
Hartquist, T. W., Williams, D. A., & Caselli, P. 1996, Ap&SS, 238, 303
Herbst, E., & Leung, C. M. 1989, ApJS, 69, 271
Howe, D. A., Millar, T. J., Schilke, P., & Walmsley, C. M. 1994, MNRAS, 267, 59
Irvine, W. M., Goldsmith, P. F., & Hjalmarson, Å. 1987, in Interstellar Processes, ed. D. J. Hollenbach & H. A. Thronson (Dordrecht: Reidel), 561
Langer, W. D. 1985, in Protostars and Planets II, ed. D. C. Black & M. S. Matthews (Tucson: Univ. Arizona Press), 650
Langer, W. D., et al. 1997, ApJ, 480, L63
Larsson, M., et al. 1996, A&A, 309, L1
Le Bourlot, J., Pineau des Forêts, G., & Roueff, E. 1995, A&A, 297, 251
Lee, H.-H., Bettens, R. P. A., & Herbst, E. 1996, A&AS, 119, 111 (LBH)
Lemme, C., Walmsley, C. M., Wilson, T. L., & Muders, D. 1995, A&A, 302, 509
Leung, C. M., Herbst, E., & Huebner, W. F. 1984, ApJS, 56, 231
Linsky, J. L., Diplas, A., Wood, B. E., Brown, A., Ayres, T. R., & Savage, B. D. 1995, ApJ, 451, 335
Lucas, R., & Liszt, H. S. 1996, in IAU Symp. 178, Molecules in Astrophysics: Probes and Processes, ed. E. F. van Dishoeck (Leiden: Sterrewacht), 421
McKee, C. F. 1989, ApJ, 345, 782
Millar, T. J., Bennett, A., & Herbst, E. 1989, ApJ, 340, 906
Millar, T. J., & Herbst, E. 1990, A&A, 231, 466
Myers, P. C., Fuller, G. A., Goodman, A., & Benson, P. J. 1991, ApJ, 376, 561
Myers, P. C., & Khersonsky, V. K. 1995, ApJ, 442, 186
Neufeld, D. A., Lepp, S., & Melnick, G. J. 1995, ApJS, 100, 132
Prasad, S. S., & Huntress, W. T. 1982, ApJ, 260, 590
Pratap, P., Dickens, J. E., Snell, R. L., Miralles, M. P., Bergin, E. A., Irvine, W. M., & Schloerb, F. P. 1997, ApJ, 486, 862
Ruffle, D. P., Hartquist, T. W., Taylor, S. D., & Williams, D. A. 1997, MNRAS, in press
Shu, F. H., Adams, F. C., & Lizano, S. 1987, ARA&A, 25, 23
Spitzer, L. 1978, Physical Processes in the Interstellar Medium (New York: Wiley)
Suzuki, H., Yamamoto, S., Ohishi, M., Kaifu, N., Ishikawa, S., Hirahara, Y., & Takano, S. 1992, ApJ, 392, 551
van Dishoeck, E. F., Blake, G. A., Draine, B. T., & Lunine, J. I. 1993, in Protostars and Planets III, ed. E. H. Levy, J. I. Lunine, & M. S. Matthews (Tucson: Univ. Arizona Press), 163
Ward-Thompson, D., Scott, P. F., Hills, R. E., & André, P. 1994, MNRAS, 268, 276
Whittet, D. C. B., et al. 1996, A&A, 315, L357
Wootten, A., Loren, R. B., & Snell, R. L. 1982, ApJ, 255, 160
Wootten, A., Snell, R., & Glassgold, A. E. 1979, ApJ, 234, 876